Travail de fin d'études et stage[BR]- Travail de fin d'études : Assessing the complementarity of CSP, PV and battery technologies in a global grid setting: methodology and preliminary results[BR]- Stage d'insertion professionnelle

Auteur : Mbenoun, Jocelyn
Promoteur(s) : Ernst, Damien
Faculté : Faculté des Sciences appliquées
Diplôme : Master en ingénieur civil électromécanicien, à finalité spécialisée en énergétique
Année académique : 2020-2021
URI/URL : http://hdl.handle.net/2268.2/11240

Assessing the complementarity of CSP, PV and battery technologies in a global grid setting: methodology and preliminary results

Master thesis realized in order to obtain the degree of master in "Civil Engineer in Electromechanics" by Jocelyn Mbenoun

Supervisor : Prof. *Damien Ernst* and Dr. *Raphaël Fonteneau*

University of Liège - Faculty of Applied Sciences
Academic year: 2020-2021

Abstract

The main objective of this study is to determine if concentrated solar power (CSP) plants with thermal energy storage (TES) are still economically viable when put in competition with PV systems and batteries for a large scale power generation in a global grid setting. Towards this goal, an optimization-based framework is implemented and exploited to identify the best combination of generation means among CSP, PV and battery to satisfy a chosen electricity demands while minimizing the levelized total system cost (LTSC). This thesis will mainly focus on a methodology to optimize the sizing of installations and the generation of electricity. The type of concentrated solar power used for this study is the parabolic trough which is, as of today, the most common and mature of all concentrated solar power plant. In order to tackle the complexity of modelling the CSP and to reduce the computation time of the optimization problem, the sizing and the generation of the CSP and PV are optimized through a hybrid heuristic technique. Indeed, from the results of simulation of a software specialized in renewable energy project, the System Advisor Model (SAM), a model using linear equations will be implemented on a python code able to solve optimization problems. The configuration of the system considers Kôm Ombo in Egypt as the installation site and the Belgium electricity demand as load. Results of the optimization show that the LCOE, the levelized cost of electricity, decreases when CSP is added to the PV-battery system. Within an investment horizon of 25 years, the LCOE drops from 110.20 $/MWh using only PVs and battery to 77.74 $/MWh for the most realistic setting. The LCOE decrease is achieved by taking advantage of the TES of the CSP which allow to generate electricity several hours after collecting energy through the solar field. These results clearly show that, under realistic capacity and cost assumptions, CSP may still be economically viable today, in particular by designing a system in which CSP and PV-battery systems play a complementary role.

Contents

List of Figures

Part I
Introduction

1 Context

One of the major challenges of the current century is the reduction of the release of greenhouse gases in the atmosphere. Their negative effects on the climate have long been proven and several countries have already agreed to drastically curb their greenhouse gas emission. However, the global electricity consumption has increased at a constant pace in previous years and is expected to keep this trend in the next decades. The World Energy Council forecasted it to grow from 22000 TWh in 2017 to 40000 TWh in 2050 [1]. With the current means of electricity production mainly burning fossil fuels, the increase in the release of carbon dioxide, a potent greenhouse gas, is unavoidable. Therefore, a considerable change in the means of production must be achieved and many climate policies aim at replacing fossil fuel-based power generation technologies with renewable ones.

Nevertheless, implementing renewable-based generation into the power system is not an easy task. The unpredictable and intermittent production patterns of technologies such as wind turbine and photovoltaic (PV) panel makes their management particularly challenging [2]. To tackle this inconvenience, the use of storage capacities has been studied. More and more models proposed a system with PV and batteries in order for the production of electricity to be able to follow a certain demand curve [3].

Another solution proposed is the development of interconnection between adjacent power systems and, by extension, the global grid concept. The idea consists in merging all power systems into one electricity transmission system covering the whole globe [4]. One of the key benefits of such a system is the possibility to harvest large quantities of energy in isolated places with abundant resources for renewable energy production and dispatch it into dense, energy-intensive and resource-limited demand centers. Several projects have been studied and even been launched in this path, such as the Desertec Project. Its aim was to harness renewable energy source from the sun in the Sahara with concentrated solar power (CSP) plants to supply the demand in Europe, North Africa and Middle East. It aspired to meet 17% of the demand of Europe in 2050 [5].

CSP plants generate power with steam turbines that provide a spinning reserve which has a key role within the electricity grid for short time compensation during an outage or a failure. Moreover, another advantage is the ability of CSP plants to operate in all load segments thanks to their flexible design. They can provide steady power capacity and act like any conventional steam cycle power station [6].

Despite its numerous benefits, CSP plants do not meet as much interest as the PV system. Financing seems to be the primary barrier in the development of CSP [8]. With the economic crisis of 2008, commercial banks and investors are no longer as eager to invest in long-term and low interest projects such as a CSP plant would require [9]. Moreover, PV systems can be built faster and at lower cost than CSP plants and their prices have substantially dropped in the last couple of years and are expected to continue to drop [7].

However, CSP plants offer the advantage of enabling the storage of the energy in a thermal state. Thermal energy storage (TES) technologies, being far more efficient than electricity storage tech-

nologies(lower losses and longer lifetime), increases the attractiveness of CSP systems for large scale power generation. According to a research conducted at the US National Renewable Energy Laboratory (NREL), the use of TES in CSP could be used as a complementary solution by smoothing out variability in production observed in the use of other renewable energy such as wind turbine or PV.

2 Objective

The main objective of this thesis is to determine if CSP plants with TES are still economically viable when put in competition with PV systems and batteries for a large scale power generation. Towards this goal, an optimization-based framework is implemented and exploited to identify the best combination of generation means among CSP, PV and battery to satisfy a chosen electricity demands while minimizing the levelized total system cost (LTSC). Moreover, the study will take place in a global grid setting where CSP and PV are installed in an isolated area with abundant resources for renewable energy to feed a highly demanding less resourceful area in electricity .

3 Overview of different technologies

This section presents an introduction about the different technologies used in the model and on how they produce electricity.

3.1 Concentrated solar power (CSP) plant

A concentrated solar power plant is a thermal power plant using mirror or lenses to focus sunlight into a receiver that will heat a fluid (liquid or gas). This fluid will then be used to produce steam that is expanded in a turbine to generate electricity. The generation of electricity being highly dependent of direct solar irradiation, only location with high solar direct normal irradiation ($\geq$ 2000 kWh/m^2/yr) are suitable for achieving attractive levelized costs of electricity (LCOE) (0.16 \$/kWh to 0.33 \$/kWh) [17]. Another requirement for CSP is the access to water resources, for cooling like other thermal plant but also to wash receiver and mirror surfaces [9]. Moreover, thermal storage can be added to produce electricity even when the sun is not present.

As of today, 4 configurations have been used to produce energy through this technology : using parabolic trough reflector, using linear fresnel reflectors, using solar tower and the Stirling dish systems. Among those 4, only the parabolic trough reflector and the solar tower configurations allow the storage and the dispatch of energy and, therefore, are relevant in this study.

3.1.1 CSP with parabolic trough reflectors

These CSP use linear parabolic reflectors and receiver in form of tube located along the reflector's focal line. Inside of the receiver, a heat transfer fluid (HTF) is heated. Depending on the nature of this fluid, it can be heated from 400°C for synthetic oil to 550°C with molten salts or direct steam [16]. The hotter the fluid is heated, the more the plant can produce electricity. In order to maximize energy harvested from the solar field, a single axis tracking system is used to move the reflectors along with the receiver attached to it to follow the sun path.

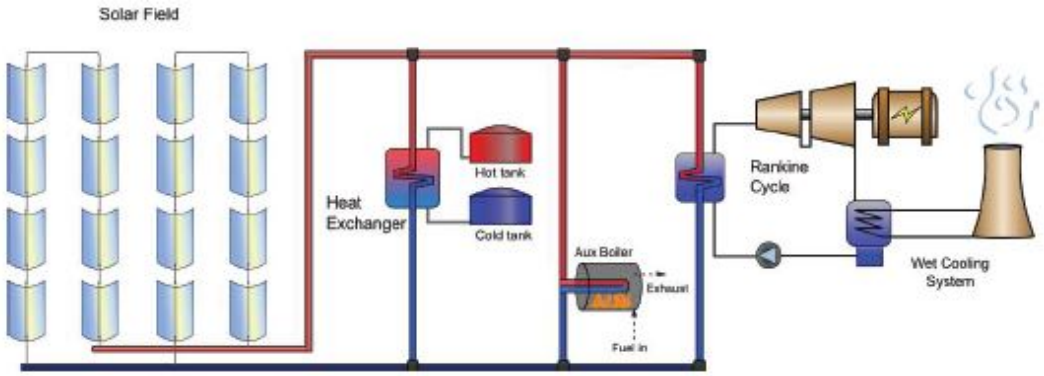

Figure 1: Schematic of a conventional parabolic trough CSP plant [12]

The HTF is then usually used to heat up water in a superheated Rankine steam cycle. The Rankine cycle is a thermodynamic cycle comprised of 4 processes : an isentropic compression, an isobaric heat addition, an isentropic expansion and an isobaric heat rejection in a condenser. When water is the working fluid such as in a Rankine steam cycle, the isentropic compression is done when the water is in its liquid form in a pump. Then, during the isobaric heat addition, the water is heated till it vaporizes. In the case of CSP, it is done through a heat exchange with the HTF during the isentropic expansion. The steam is then expanded in a turbine to produce mechanical power. If the turbine is connected to a generator, electricity can be generated. Finally, the steam is condensed into water to close the cycle and be pumped again. In a superheated Rankine cycle, the steam is heated above its boiling temperature before being expanded in order to avoid the formation of droplet of water during the expansion that may damage the turbine. In the parabolic trough CSP plant, the steam can reach temperature from 380°C to 540°C at 100 bar depending on the transfer fluid used [17].

Finally, a thermal storage can be added in order to store and dispatch thermal energy from a few minutes to a day's worth. Composed of 2 tanks, one to store the thermal fluid at low temperature and the other to store it at high temperature, 2 types of storage exist: the direct storage and the indirect storage. For the direct storage, the HTF is also used as the thermal storage. Once heated, a fraction of HTF is stored while the other is used to produce steam in the Rankine cycle. For the indirect storage, the HTF is not the same as the thermal storage. A heat exchanger is added to transfer energy between the thermal storage fluid and the HTF. This approach can be used when expensive oil are used as the HTF. Molten salt or cheaper oil can therefore be used in the storage system to decrease the overall cost of the plant [12].

Typical capacity of CSP with parabolic trough collectors ranges from 10 to 300 MW, its annual solar-to-electricity efficiency from 11 to 16 % and its plant peak efficiency from 14 to 20 % [17]. As of today, it is the most common type of CSP installed in the world, accounting for 90 % of total CSP systems due to its technology being the most mature and has been used since decades [21]. It is also possible to include a fossil-fuel heater to provide additional energy in case of lack of solar radiation [12]. Additionally, CSP using parabolic trough can also be integrated into a fossil-fired plant to decrease the use of fuel [19].

3.1.2 The Solar Tower

Solar towers use a field of heliostats (dual-axis tracked mirrors) to concentrate solar radiation onto a receiver at the top of a tower. Depending on the fluid used as the HTF, the upper working temperature varies between 250 and 1000°C for future plant [17]. Molten salt, water/steam and air (at atmospheric pressure or pressurized ($\sim$ 15 bar) [18]) are the fluids used to transport the heat.

The HTF either produces steam thanks to a heat exchanger in a superheated Rankine cycle whether molten salt or air is used, or is directly used in the Rankine cycle when steam is used as the HTF. The steam can be heated at 540°C with pressure varying from 100 to 160 bar depending on the nature of HTF [18]. Hybridization with a fossil-fired plant and or a duct burner to heat up the HTF are possible when using air as the HTF fluid.

Solar tower with molten salt central receiver can also used a direct thermal storage to increase the capacity factor of the plant. Like with parabolic trough collectors, it is composed of 2 tanks, one to store the thermal fluid at the upper working temperature (550°C) and the other at a lower temperature (250°C) [18].

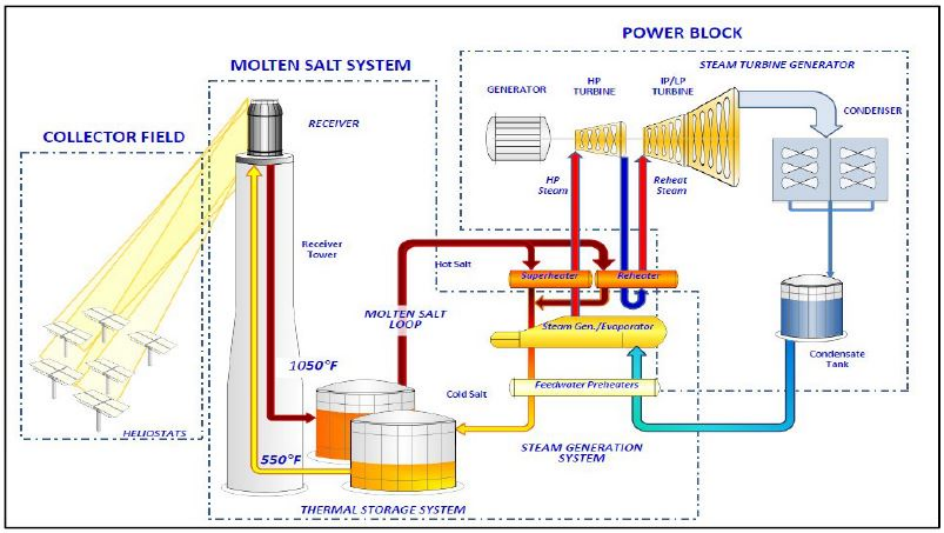

Figure 2: Schematic of a conventional solar tower using molten salt and with direct thermal storage [18]

Typical capacity of CSP using solar tower ranges from 10 to 200 MW, its annual solar-to-electricity efficiency from 7 to 20 % and its plant peak efficiency from 23 to 35 % in a combined cycle turbine. Despite not being the most common type of CSP installed in the world, it is the most promising. The higher temperatures can increase the efficiency of the steam cycle, reduce water consumption for cooling steam in the condenser, make the use of thermal storage more attractive by allowing greater temperature differentials in the storage system, reducing costs or allowing greater storage for the same

cost [17].

3.2 Solar panels (PVs)

3.2.1 Energy production from photocell

PVs are made of photocells. Photocells are composed of semiconducting materials able to convert incidents photons into electric energy. Depending on the energy of the photon incident (and therefore its wavelength), electrons can be freed from their atom. In order to generate a current, free electrons are collected using 2 semi-conductors doped differently:

- one semiconducting material of n-type that gives an excess of electron once photons reach it
- another semiconducting material of p-type that gives a default of electron once photons reach it

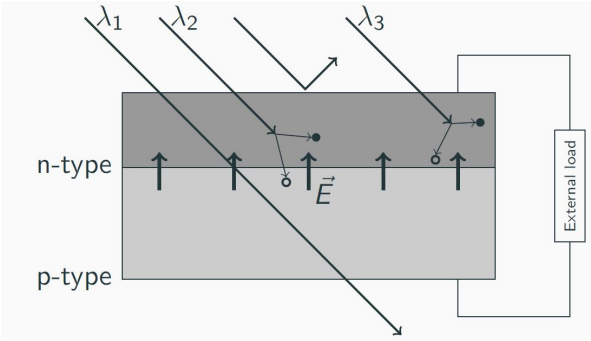

Figure 3: Schematic of a photocell [10]

Connecting both materials, an electric field $\overrightarrow{E}$ is then created and a current can be generated as seen in Figure 3.

3.2.2 Types of PV Cells and efficiency

Photocells don't all use the same semiconductors to produce electricity. The 4 most common types of cells are the silicon (Si) cells, the amorphous silicon (aSI:H) cells, the gallium arsenide (GaAs) cells and the copper indium (gallium) selenide (CIGS) cells [10]. Depending on the materials used, the efficiency, the lifetime and the price of the PVs vary:

- Silicon cells have a 20 years lifetime and efficiency of 20% for monocrystalline type but the silicon production is very energy intensive (200 kWh/kg) [10]. Polycrystalline type were developed to decrease the demand of energy to produce silicon cells but their efficiency only reaches 15 to 16%.
- Amorphous silicon cells are cheaper to produce and can be used to produce thin film PV panels but their efficiency only reaches 10% for industrial use and they have a limited lifetime [10].
- Gallium Arsenide cells can also be used to produce thin film PV panels, are very efficient (up to 30%) and have a very long lifetime but are expensive to produce. They are mostly used for spatial application.

- Copper indium (Gallium) Selenide cells have an intermediate efficiency of 13 % for industrial use, are cheap to produce since most components are easily available and can be used to produce thin film PV panels.

3.3 Lithium-ion (Li-Ion) Batteries

The most common battery used to store electricity produced by PV panels is the Li-Ion battery. It is a solid-state battery that stores energy in electrochemical form. The main characteristic of Li-Ion battery is its high specific energy. It also exhibits a higher energy and power density than other battery technologies, possesses a high rate and high power discharge capability, one of the best round-trip efficiency (between 85 and 96%), a low self-discharge rate and a rather long lifetime (5 to 20 years) [3].

Lithium ions are used to charge battery cells within the battery in electrodes through a redox reaction. Each cell is composed of 2 electrodes: a positive one called cathode made of a compound of metal oxide and lithium and a negative one called anode made of a compound of graphite matrix and lithium too. Both electrode are connected to each other through an external circuit and are both emerged in an electrolyte. When the battery is charging, electrons move from the cathode to the anode through the external circuit while positive charged lithium ions leave the cathode during an oxidation half-reaction through the electrolyte. Lithium ions are then attached to the anode with electrons coming from the external circuit in a reduction half reaction and the energy is stored as chemical energy as seen in Figure 4.

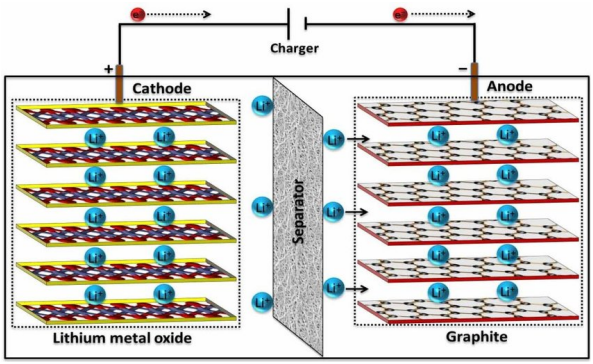

Figure 4: Schematic of a photocell [11]

When the battery is discharging, electrons move in the opposite direction, from the anode to the cathode. Lithium cations leave the anode and are combined to the cathode with the electrons coming from the external circuit. The chemical potential of the cell is diminished since the energy is transferred from the cell to the external circuit.

One of the main issues that needs to be monitored is the release of oxygen during chemical reaction when the cathodes overheat. In this situation, leaks and smoke gas venting could occur and lead to the cell catching fire. In order to avoid it, thermal management and monitoring processes are integrated in the Li-ion battery energy storage system. They also serve to regulate the operating temperature of the battery since it has a significant impact on performance and cycle lifetime.

Part II
Methodology

This study will mainly focus on a methodology to optimize the sizing of installations and the generation of electricity. The model will be realized to meet the demand of Belgium for the year 2019 using linear programming. The type of concentrated solar power used for this study is the parabolic trough which is as of today, the most common and mature of all concentrated solar power plant.

4 Choice of place for the installations

As a reminder, the location chosen for the installation of the CSP must display a high solar direct normal irradiation, of at least 2000 kWh/m^2/yr and have an access for water in order to be able to cool down the plant and to wash the receiver and mirror surfaces. Therefore, the Sahara was chosen as the location, and more precisely, a site located close to Kôm Ombo in Egypt. It possesses an annual solar direct normal irradiation of almost 2600 kWh/m^2 [15] and an easy access to water resources since the city of Kôm Ombo is located on the right bank of the Nile. A 100 MW CSP has already been installed led by the New & Renewable Energy Authority (NREA) [24].

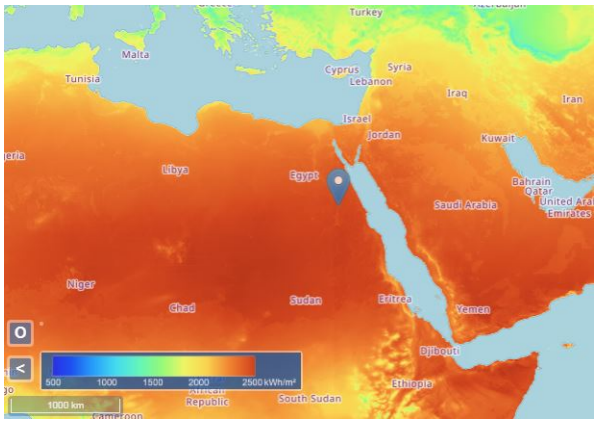

Figure 5: Location chosen for the installation of CSP

5 CSP plants, PVs and batteries sizing and generation

In order to tackle the complexity of modelling the CSP and to reduce the computation time of the optimization problem, the sizing and the generation of the CSP and PV are optimized through a hybrid heuristic technique. Indeed, from the results of simulation of a software specialized in renewable energy project, a model using linear equations will be implemented on a code written in python able to solve optimization problems. Using the software System Advisor Model (SAM), the generation potential of the CSP and PV will be evaluated at different operating conditions that will serve as references in the

sizing problem and approximations for the generation simulations.

Developed and distributed by the U.S. Department of Energy's National Renewable Energy Laboratory (NREL), SAM is a open source program that allows to calculates performance and financial metrics of renewable energy projects from an hourly simulation engine. SAM is a reliable software, well documented and has been used in many researches about renewable energy.

The objective is to model the sizing and the generation of each technology as a set of linear equations from the analysis of simulations produced by SAM. Then, those linear equations will be used in a mathematical linear program to determine the best combination of generations means. In a linear program, also called linear optimization, the function to optimize and all the constraints are linear. Equation (1) represents a linear program in standard form.

$$\begin{aligned} &\min\ c^T x \\ &s.t.\ Ax = b \\ &x \in \mathbb{R}^n_+ \end{aligned} \tag{1}$$

Costs for CSP and PVs will be computed from equations used in the SAM software. Further explanations will be given in the following sections. As for the battery, its characteristics such as the round-trip efficiency, lifetime and prices will be taken from the literature.

Part III
System Advisor Model (SAM)

In order to simulate the concentrated solar power plant and PV panels production, the System Advisor Model assigns values to input variables to provide information about the project's location, type of equipment in the system, cost of installing and operating the system and financial and incentives assumptions. This part presents the most important parameters that have been set and variables that will be studied within the software for the CSP and PV. The system performance is then modeled using the TRNSYS software, a time-series simulation program developed at the University of Wisconsin, integrated into SAM.

Moreover, SAM is regularly updated by the NREL to keep track with the technological advancement of different renewable energy sources and correct possible errors of the software. Therefore, defaults values used by software are realistic since there are based on existing projects.

6 CSP with parabolic trough in SAM

SAM propose 2 models to simulate a parabolic trough system, the physical trough model and the empirical trough model. Both models determine the electricity delivered to the grid. While the physical trough system model evaluates the performance of different components of the system using first principles of heat transfer and thermodynamics, the empirical trough model use empirical measurements from the SEGS projects, a CSP plant in California [22]. Despite the fact that the physical trough model adds more uncertainty to performance predictions than the empirical model, it is more flexible since it is suitable for most systems. The empirical model can only be used for design similar to the SEGS projects. Therefore, this is the physical trough that is described and used in this study.

6.1 Introduction

CSP with parabolic trough can be divided in 3 distinctive parts: the solar field, the power cycle and the thermal storage. The solar field collects the heat required to power the plant. It is composed of collector assemblies (SCA's) arranged in one or more loops laid out in parallel and header pipes. Each SCA is composed of parabolic collectors and their receivers in series. The header pipes which transfer the HTF between the power cycle or the thermal storage and the solar field.

The power cycle is the part of the plant that converts the thermal energy from the solar field into useful mechanical or electricity energy. It most often uses a Rankine cycle and electric generator although other approaches exist.

Finally, the thermal storage subsystem is composed of tanks and heat exchangers to store and dispatch thermal energy from a few minutes to a day's worth. In some cases, a fossil-fuel heater is also included to provide supplemental energy.

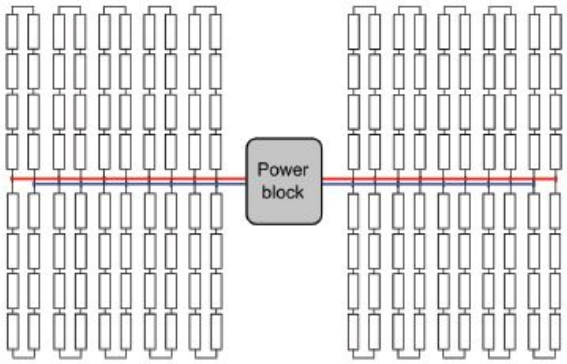

Figure 6: Example of a solar field of 20 loops where each loop contains 8 SCA's and divided into 2 header sections. The blue lines represent the header pipes providing the "cold" HTF from the power cycle to the solar field and the red lines represent the header pipes collecting the "hot" HTF from the solar field to the power cycle. [12]

6.2 Parameters of the model

6.2.1 Solar field

In order to size the solar field to meet the requirements to produce enough thermal energy, some parameters need to be set. First of all, the type of collectors and receivers that will be used need to be chosen and with it, the associated parameters. SAM proposes a set of collector and receiver parameters for several commercially available collectors and receivers. In this study, the collector used is the SkyFuel's SkyTrough and the receiver used is the Schott PTR80.

For the collectors, there are 2 types of parameters: the collector geometry parameters and the optical parameters. While the collector geometry parameters define the size of the collector, setting the reflective aperture area, A_{SCA}, and the length of a collector assembly as example, the optical parameters account for the efficiency of the collector performance.

The other optical parameters are the tracking error η_{track}, that account for the imperfect orientation of the collector along the tracking angle, the geometry defects η_{geo}, the mirror reflectance ρ_m, the mirror soiling η_{soil} and the general error η_{gen} that account for any effect that is not taking into account by the previous parameters. Using these parameters, the optical efficiency of the collector at design $\eta_{opt,design}$ can be deducted:

$$\eta_{opt,design} = \eta_{track} \times \eta_{geo} \times \rho_m \times \eta_{soil} \times \eta_{gen} \tag{2}$$

Table 1 provides the values of each parameters related to the collectors for SkyFuel's SkyTrough parabolic collector. Moreover, to take into account the arid climate of the location chosen, a mirror soiling of 0.834 based on the research made by A. Azouzoutea, A. Alami Merrounia, M. Garoumb [27] on the effect of soiling on the performance of mirror.

Parameters	Notation	Value	Unit
General error	η_{gen}	1	-
Geometry defects	η_{geo}	0.952	-
Tracking error	η_{track}	0.988	-
Mirror reflectance	ρ_m	0.93	-
Mirror soiling	η_{soil}	0.834	-
Reflective aperture area	A_{SCA}	656	m^2

Table 1: Parameters related to the collector and their values for the SkyFuel SkyThrough [13]

As for the receiver, it comprises 2 parts: the absorber and the glass envelope. The heat transfer fluid used to harvest the thermal energy flows through the absorber while the glass envelope allows to enclose vacuum around it. The receiver geometry is defined by setting the absorber tube and the glass envelope inner and outer diameters, $D_{abs,in}$, $D_{abs,out}$, $D_{gl,in}$, $D_{gl,out}$, the internal surface roughness of the absorber and the absorber material type. Figure 7 presents a schematic of the collector and receiver and Table 2 the values of their diameters given by the data set of SAM.

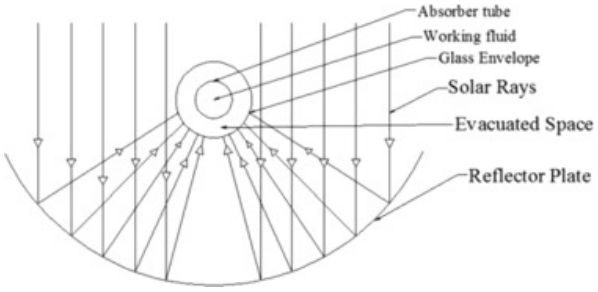

Figure 7: Schematic of the collector and receiver [23]

Parameters	Notation	Value	Unit
Absorber tube inner diameter	$D_{abs,in}$	0.076	m
Absorber tube outer diameter	$D_{abs,out}$	0.08	m
Glass enveloppe inner diameter	$D_{gl,in}$	0.115	m
Glass enveloppe outer diameter	$D_{gl,out}$	0.12	m

Table 2: Sizing parameters for the Schott PTR80 receiver [13]

The other parameters to set are the absorber absorptance α_{abs}, absorber emittance ϵ_{abs}(which can be set at different values depending on the surface temperature of the absorber), the envelope absorptance α_{env} , the envelope emittance ϵ_{env}, the envelope transmittance τ_{env}, the estimated heat average heat loss $\dot{q}_{hl}$ and the optical effects such as the bellows shadowing $\eta_{bellows}$ and the dirt on receiver η_{dirt}. Moreover, different conditions of the receiver type can be described, called variations. For example, a variation can be used to describe the receiver in good condition and another one to describe a degraded receiver, with a damaged glass envelope for example. Each variation is associated to a variant weighting fraction, f_{weight}, that describes the fraction of the solar field that operate at the conditions of this variation. Up to 4 different variations can be defined. Values of those parameters are presented in Table 3 and Table 4 for the Schott PTR80 receiver. Based on default values of SAM, only 3 variations are used for this receiver. As for the effect of dirt on receiver, no research has been found on that matter. Most researches focus on heat losses since it is the principal cause of loss of performance in the receiver. A value of 0.9 has been chosen but further researches and experiments should be conduct about it.

Parameters	Notation	Values			Unit
Variant weighting fraction	f_{weight}	0.985	0.01	0.005	-
Broken glass enveloppe	-	No	No	Yes	-

Annulus gas type	-	Hydrogen	Air	Air	-
Absorber absorptance	α_{abs}	0.963	0.963	0.8	-
Envelope absorptance	α_{env}	0.02	0.02	0	-
Absorber emittance	ϵ_{abs}	See Table 4	0.65	0.65	-
Envelope emittance	ϵ_{env}	0.86	0.86	1	-
Effect of bellows shadowing	$\eta_{bellows}$	0.935	0.935	0.935	-
Effect of dirt on receiver	η_{dirt}	0.9	0.9	1	-
Envelope transmittance	τ_{env}	0.964	0.964	1	-
Estimated heat average heat loss	$\dot{q}_{hl}$	190	1270	1500	W/m

Table 3: Parameters related to the receiver and values for the Schott PTR80 receiver [13]

Surface Temperature (°C)	100	150	200	250	300	350	400	450	500
Absorber emittance	0.064	0.0665	0.07	0.0745	0.08	0.0865	0.094	0.1025	0.112

Table 4: Absorber emittance of receiver for $f_{weight} = 0.985$ [13]

From the receiver parameters, the heat loss at design and the optical derate of the receiver representing the total optical losses expected from the receiver can be computed :

$$\dot{Q}_{hl,design} = \sum_{i=1}^{4} f_{weight,i} \times \dot{q}_{hl,i} \tag{3}$$

$$\eta_{opt,derate} = \sum_{i=1}^{4} f_{weight,i} \times \eta_{bellows,i} \times \eta_{dirt,i} \times \alpha_{absorb,i} \times \tau_{env,i} \tag{4}$$

Coupling the collector and the receiver together, the loop optical efficiency when incident radiation is normal to the aperture plane can be computed

$$\eta_{opt,loop} = \eta_{opt,design} \times \eta_{opt,derate} \tag{5}$$

Then using the heat loss at design to calculate the receiver heat loss efficiency $\eta_{hl,loop}$, the total loop conversion efficiency is computed

$$\eta_{conv,loop} = \eta_{opt,loop} \times \eta_{hl,loop} \tag{6}$$

Parameters implied	**Notation**	**Value**	**Unit**
Optical efficiency of the collector at design	$\eta_{opt,design}$	0.73	-
Optical derate of the receiver	$\eta_{opt,derate}$	0.78	-
Heat loss at design	$\dot{Q}_{hl,design}$	207.35	W/m
Loop optical efficiency	$\eta_{opt,loop}$	0.57	-
Total loop conversion efficiency	$\eta_{conv,loop}$	0.55	-

Table 5: Parameters implied for the collector and the receiver

Important remaining parameters to set include the row spacing between loops L_{row}, the aperture width W_{sca}, the number of SCA's per loop which allows to calculate the single loop aperture

$$A_{loop} = N_{SCA} \times A_{SCA}, \tag{7}$$

the number of field subsections as seen in Figure 8 that defines the location and the shape of header piping which affects the heat loss calculations and the power consumed by the pumps in the solar field, the heat transfer fluid (HTF) and its properties, especially its minimum and maximum operating temperature. Table 6 presents the values of parameters relative to the sizing of a loop of the solar field based on the default values of SAM.

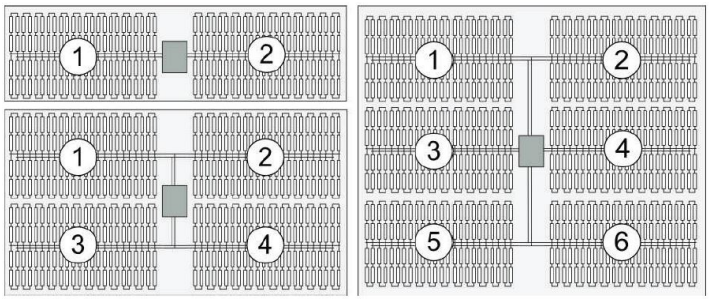

Figure 8: Different configurations of the solar field depending on the number of field subsections. 2 field subsections have been chosen for the configuration in the top left, 4 in the bottom left and 6 on the right [12]

Parameters	Notation	Value	Unit
Row spacing	L_{row}	15	m
Aperture width	W_{sca}	6	m
Number of SCA's per loop	N_{SCA}	8	-
Single loop aperture	A_{loop}	5248	m^2
Number of field subsections	N_{sub}	2	-

Table 6: Sizing parameters of the loop [13]

The freeze minimum temperature, meaning the minimum temperature the heat transfer fluid is allowed to reach in the field, the design temperature at the inlet and outlet of the loop and the minimum and maximum single loop flow rate, $\dot{m}_{loop,min}$ and $\dot{m}_{loop,max}$ which allows to compute the minimum and maximum field flow velocity using Equations (8) and (9) are important parameters that delimit the performances of the CSP.

$$v_{min} = \frac{\dot{m}_{loop,min} \times 4}{\rho_{HTF,in} \times \pi \times D^2_{abs,in}} \tag{8}$$

$$v_{max} = \frac{\dot{m}_{loop,max} \times 4}{\rho_{HTF,out} \times \pi \times D^2_{abs,in}} \tag{9}$$

where $\rho_{HTF,in}$ is the density of the heat transfer fluid at the design inlet temperature and $\rho_{HTF,out}$ is the density at the design outlet temperature.

The heat transfer fluid chosen for this study is the Therminol VP-1 which is a ultra high temperature synthetic heat transfer fluid. A key advantage of this fluid is its superb heat transfer properties. Indeed, the Therminol VP-1 has the highest thermal stability (which is the ability of a fluid to resist breaking down under heat stress), a low viscosity and a wide temperature use range of 12°C to 400 °C [25]. The values used for the parameters related to the heat transfer fluid are presented in Table 7 based on SAM default values.

Parameters	**Notation**	**Value**	**Unit**
HTF	-	Therminol VP-1	-
Loop inlet HTF temperature	$T_{HTF,in}$	293	°C
Loop outlet HTF temperature	$T_{HTF,out}$	393	°C
Maximum single loop flow rate	$\dot{m}_{loop,max}$	1	kg/sec
Minimum single loop flow rate	$\dot{m}_{loop,min}$	12	kg/sec
Density of the HTF at $T_{HTF,in}$	$\rho_{HTF,in}$	820.811	kg/m^3
Density of the HTF at $T_{HTF,out}$	$\rho_{HTF,out}$	706.384	kg/m^3
Maximum field flow velocity	$\dot{v}_{max}$	0.3	m/sec
Minimum field flow velocity	$\dot{v}_{min}$	3.7	m/sec

Table 7: Parameters related to the HTF [13]

6.2.2 Power Cycle

The parameters of the Power Cycle can be divided into 3 categories, the system design parameters, the general design parameters and the Rankine cycle parameters. The system design parameters account for the estimated gross to net conversion factor $\eta_{pc,gtn}$ and the cycle thermal efficiency $\eta_{pc,th}$. The estimated gross to net conversion factor is the ratio between the net amount of electric energy delivered to the network and the power cycle gross power produced while the cycle thermal efficiency is the ratio between the thermal power delivered to the power cycle and the turbine gross output under design conditions [14].

The general design parameters take into account the fraction of the thermal power needed by the power cycle to remain in standby $\zeta_{th,standby}$ and for startup $\zeta_{th,startup}$, the power block startup time $t_{startup}$, the minimum and the maximum turbine operation point $\zeta_{min,turb}$, $\zeta_{max,turb}$, both as fraction of the nameplate electric capacity of the power cycle and the pumping power for HTF through power block [14].

Finally, the most important parameters of the Rankine cycle are the boiler operating pressure and the condenser type. SAM gives the choice between 4 types of condenser type : evaporative, air cooled, hybrid (evaporative and air cooled in parallel) and radiative. Table 8 presents the values and units of the power cycle parameters. Realistic defaults values given by the software have been used.

System design parameters	**Notation**	**Value**	**Unit**
Estimated gross to net conversion factor	$\eta_{pc,gtn}$	0.9	-

Cycle thermal efficiency	$\eta_{pc,th}$	0.356	-
General design parameters	**Notation**	**Value**	**Unit**
Maximum turbine operation point	$\zeta_{max,turb}$	1	-
Minimum turbine operation point	$\zeta_{min,turb}$	0.2	-
Fraction of the thermal power for standby	$\zeta_{th,standby}$	0.2	-
Fraction of the thermal power for startup	$\zeta_{th,startup}$	0.2	-
Power block startup time	$t_{startup}$	0.5	hours
Pumping power for HTF through power block	-	0.55	kW/kg/s
Rankine cycle parameters	**Notation**	**Value**	**Unit**
Boiling operature pressure	-	100	bar
Condenser type	-	Evaporative	-

Table 8: Parameters used for the power cycle and their values [13]

6.2.3 Thermal storage

In order to set the thermal storage subsystem, the storage heat transfer fluid need to be chosen. Moreover, parameters concerning the geometry of the tanks and its properties such as the number of tanks pairs $N_{tank,pair}$ (the hot and the cold tanks), their height H_{tank} (all tanks have the same), their thermal loss coefficient $h_{tank,loss}$ need to set.

The remaining parameters take into account the minimum temperatures allow in the cold $T_{tank,cold,min}$ and hot tank $T_{tank,hot,min}$, the heaters capacity $\dot{W}_{heater}$ that are used to avoid falling below those temperature and the initial state of the thermal storage and their efficiency η_{heater}.

Hitec Solar Salt was chosen as the storage heat transfer fluid. It is a molten salt composed of $NaNO_3$ at 60 % and KNO_3 at 40 % and it is one of the cheapest molten salt available at 0.49 $/kg [26]. Table 9 presents the values and units of the thermal storage parameters. Like with the power cycle, realistic defaults values given by the software have been used.

Parameters Set	**Notation**	**Value**	**Unit**
Storage HTF	-	Hitec Solar Salt	-
Heater efficiency	η_{heater}	0.98	-
Tank thermal loss coefficient	$h_{tank,loss}$	0.4	Wt/m^2K
Tank height	H_{tank}	12	m
Number of tanks pairs	$N_{tank,pair}$	1	-
Cold tank minimum temperature	$T_{tank,cold,min}$	250	°C
Hot tank minimum temperature	$T_{tank,hot,min}$	365	°C
Heater capacity	$\dot{W}_{heater}$	25	Mwe

Table 9: Parameters used for the thermal storage and their values [13]

6.3 Variables of the model

To link the 3 parts of the concentrated solar power plant together, 4 variables are used : the design turbine gross output $\dot{W}_{des,gross}$, the solar multiple SM, the design point direct normal radiation DNI and the hours of storage at the design point of the plant $t_{full,load}$. The objective of the model is to tune this 4 variables in order to meet the electricity demand requirements taking into account the solar resource at a certain location.

The design turbine gross output is the power cycle's design output without accounting for the parasitic losses. The solar multiple is a measure of the solar field aperture area expressed as a multiple of the aperture area needed to operate the power cycle at its design capacity, when it is subjected to a constant radiation of DNI. Finally, the $t_{full,load}$ is a measure of the capacity of the thermal storage expressed in the number of hours it can deliver thermal energy at the design power cycle thermal energy.

Variables	**Notation**	**Unit**
Design point direct normal radiation	DNI	W/m^2
Solar multiple	SM	-
Storage at the design point	$t_{full,load}$	hours
Design turbine gross output	$\dot{W}_{des,gross}$	MWe

Table 10: Variables used for the model and their units

6.3.1 Power cycle

From the design turbine gross output and using the estimated gross to net conversion factor, the power cycle's nameplate capacity is calculated. It is the estimated net electric power generated by the turbine when operating at design point.

$$\dot{W}_{des,net} = \eta_{pc,gtn} \cdot \dot{W}_{des,gross} \tag{10}$$

The cycle thermal power at design can also computed using the cycle thermal efficiency

$$\dot{Q}_{th,pc} = \frac{\dot{W}_{des,gross}}{\eta_{pc,th}} \tag{11}$$

And with $\dot{Q}_{th,pc}$, the HTF mass flow rate at the design point is obtained

$$\dot{m}_{HTF,des} = \frac{\dot{Q}_{th,pc} \cdot 1000}{cp_{htf,av} \cdot (T_{loop,out} - T_{loop,in})} \tag{12}$$

The units of each variables of the power cycle are presented in Table 11

6.3.2 Solar field

From the solar multiple, the design gross turbine gross output and the irradiation at design, the total land area of the solar field can be computed.

Variables implied	Notation	Unit
HTF mass flow rate at design	$\dot{m}_{HTF,des}$	kg/s
Cycle thermal power at design	$\dot{Q}_{th,pc}$	MWt
Power cycle's nameplate capacity	$\dot{W}_{des,net}$	MWe

Table 11: Variables implied in power cycle and their units

First, the total required aperture area for a solar multiple equals to 1 is computed using

$$A_{tot,SCA,SM=1} = \frac{\dot{Q}_{th,pc}}{\eta_{conv,loop} \cdot DNI} \cdot 1e6 \tag{13}$$

From it, the number of loops needed for the solar field can be calculated :

$$N_{loop} = round\left(SM \cdot \frac{A_{tot,SCA,SM=1}}{A_{loop}}\right) \tag{14}$$

Once N_{loop} known, the total aperture reflective area can be derived

$$A_{tot,SCA} = N_{loop} \cdot A_{loop} \tag{15}$$

Taking into account the row spacing, the solar field total area is found using

$$A_{sf} = A_{tot,SCA} \cdot \frac{L_{row}}{W_{sca}} \tag{16}$$

Finally, using a non-solar field land area multiplier $\eta_{non,sf}$, which expresses the land area required by the rest of the power plant as a fraction of $A_{tot,loop}$, the total land area of the plant is obtained

$$A_{csp} = A_{sf} \cdot (1 + \eta_{non,sf}) \tag{17}$$

Moreover, the actual field thermal output at design can be derived

$$\dot{Q}_{sf,th} = \eta_{conv,loop} \cdot DNI \cdot A_{tot,SCA} \cdot 10^{-6} \tag{18}$$

The units of each variables of the solar field are presented in Table 12.

Variables implied	Notation	Unit
Total land area of the plant	A_{csp}	m^2
Solar field total area	A_{sf}	m^2
Total required aperture for SM = 1	$A_{tot,SCA,SM=1}$	m^2
Total aperture reflective area	$A_{tot,SCA}$	m^2
Number of loops	N_{loop}	-
Thermal output power	$\dot{Q}_{sf,th}$	MWt

Table 12: Variables implied in the solar field and their units

6.3.3 Thermal storage

From the number of hours of storage and the design turbine gross output, the energy capacity of the thermal storage is obtained

$$C_{tes} = \frac{\dot{W}_{des,gross}}{\eta_{pc,th}} \cdot t_{full,load} \tag{19}$$

The storage volume can then be derived

$$V_{tes} = \frac{C_{tes} \cdot 1e6 \cdot 3600}{\rho_{HTF} \cdot c_{HTF} \cdot 1000 \cdot \mu_{hx} \cdot ((T_{sf,out} - T_{hx,hot}) - (T_{sf,in} - T_{hx,cold}))} \tag{20}$$

Using the height of tank set previously, the diameter of each tank is computed

$$D_{tank} = 2 \cdot \sqrt{\frac{V_{tes}}{h_{tank} \cdot \pi \cdot N_{pair}}} \tag{21}$$

Finally, an estimated value of heat loss from all storage can be computed, assuming that the tanks are 50 % charged

$$hl_{tes} = \left(H_{tank} \cdot \pi \cdot D_{tank} + \pi \cdot \left(\frac{D_{tank}}{2} \right) \right) \cdot N_{pair} \cdot (T_{TES,ave} - 20) \cdot h_{tank,loss} \tag{22}$$

where $T_{TES,ave}$ is the average temperature of the hot and cold tanks in Kelvin, where the temperature in hot tank is equal to the solar field outlet temperature and the temperature in the cold tank is equal to the solar field inlet temperature. The units of each variables of the thermal storage are presented in Table 13.

Variables implied	Notation	Unit
Energy capacity of the thermal storage	C_{tes}	MWht
Diameter of each tank	D_{tank}	m
Estimated value of heat loss from all storage	hl_{tes}	MWt
Storage volume	V_{tes}	m^3

Table 13: Variables implied in the thermal storage and their units

7 PV in SAM

SAM propose 2 models to simulate flat plate PV systems : the detailed photovoltaic model, the PVWatts model. While the detailed photovoltaic model uses separate module and inverter models, the PVWatts model makes internal assumptions about module and inverter characteristics for three types of modules [14]. Therefore, the PVWatts model was chosen since it can simulate a reasonable estimate of a photovoltaic system's electrical output without detailed information about the equipment used in the system.

7.1 Parameters of the model

7.1.1 System parameters

As stated earlier, the PVWatts model enables to chose among 3 types of module presented in Table 14. The premium type was chosen since it possesses the highest approximate nominal efficiency. Other parameters to set include the DC to AC ratio, the ratio of the inverter's AC rated size to the array's DC rated sized and the inverter efficiency. Based on SAM default values, the DC to AC ratio is fixed at 1.1 while the inverter efficiency is fixed at 96%.

Module Type	**Approximate Nominale Efficiency**	**Module Cover**	**Temperature coefficient of power**
Standard (crystalline Silicon)	17 %	Glass	-0.47 %/°C
Premium (crystalline Silicon)	20.1 %	Anti-reflective	-0.35 %/°C
Thin film	15.6 %	Glass	-0.20 %/°C

Table 14: Types of module in SAM and their properties [14]

7.1.2 Orientation and tracking

SAM allows to chose between array types that defines if the PV modules in the array are fixed or if they move to track the movement of the sun with one or two axes of rotation. A 1-axis tracking PV array was chosen since it is, as today, the most common, cost-effective and reliable tracker. Moreover, PV modules with a single-axis tracking system can produce up to 30 % more electricity than a fixed PV modules of the same size array for a 15 to 20 % of overall system costs increase [28]. The tilt angle of solar panel, the angle between the solar panel and the horizontal plane, was set at 33 degrees and the azimuth at 180 degrees, meaning that the panels always face south as shown in Figure 9.

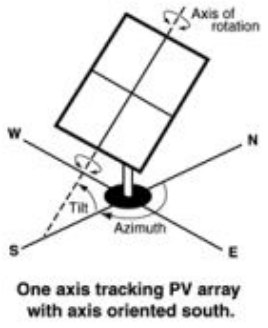

Figure 9: One axis tracking PV array with axis oriented south [14]

7.1.3 Losses

To take into account loss due to arid climate, soiling losses were set at 8 %. Other losses such as shading losses, mismatch losses caused by manufacturing imperfection between modules, wiring losses

which are resistive losses in the DC and AC wires, connections losses in electrical connectors and other were also taken into account. Their default values were used and are presented in Table 15.

Losses	Notation	Values (in %)
Soiling	$\eta_{soil,PV}$	8
Shading	η_{shad}	3
Mismatch	η_{mism}	2
Wiring	η_{wiring}	2
Connections	η_{conn}	0.5
Light-induced degradation	$\eta_{light,ind}$	1.5
Nameplate	η_{name}	1
Age	η_{age}	0
Availability	η_{avail}	3
Total system losses	$\eta_{total,syst}$	19.34

Table 15: Losses related to the solar panel

The total system losses is calculated from Equation (23).

$$\begin{aligned}\eta_{total,syst} = 1-[&(1-\eta_{soil,PV})\cdot(1-\eta_{shad})\cdot(1-\eta_{mism})\cdot(1-\eta_{wiring})\cdot(1-\eta_{conn})\\ &\cdot(1-\eta_{soil,PV})\cdot(1-\eta_{light,ind})\cdot(1-\eta_{name})\cdot(1-\eta_{age})\cdot(1-\eta_{avail})]\end{aligned} \tag{23}$$

7.2 Variables of the model

The only variable of the PV model is the system nameplate capacity in kWdc. It can be describe as the direct current power rating of the photovoltaic array in kilowatts at standard test conditions [14].

8 Weather data used by SAM

Once the CSP and PV have been designed, SAM used the data from a weather file to calculate the power generated at a particular location for a period of at least one year. Files with the appropriate file format can be downloaded from the software or from the photovoltaic geographical information system provided on the European Commission site [15] if the desired location is not available in the software. The different data elements available in the file are presented in Table 16.

For the CSP, only the direct normal irradiation is used among the irradiation elements. The albedo, the wind direction and the snow depth are not used either. As for the PV, the direct normal, the diffuse horizontal and global horizontal irradiance are used. Only the dew point temperature, the wet bulb temperature, the relative humidity and the wind direction are not used.

Data elements	**Unit**
Latitude of the location	°
Longitude of the location	°
Elevation above sea level	m
Hour of the day	Y-M-D-hh:mm
Diffuse horizontal irradiance	W/m^2
Direct normal irradiance	W/m^2
Global horizontal irradiance	W/m^2
Albedo	-
Atmospheric pressure	mbar
Dry bulb temperature	°C
Wet bulb temperature	°C
Relative humidity	%
Wind velocity	m/s
Wind direction	°
Snow depth	cm

Table 16: Weather data elements and their unit [13]

Part IV
Data analysis and linearization

One of the objective of this part is to assess the generation potential of CSP and PV from results of simulations using SAM. To do so, simulations will be done for different specific operating conditions. Moreover, for the CSP, their results will be thoroughly studied to understand relations between each component (the solar field, the power block and the thermal storage) and introduce additional hypotheses to define those relations as a set of linear equations.

The other objective is to be able to model the generations of electricity when operating conditions differ from the specific used to assess the generation potential. A study will be carry to understand how each sizing variables affect the electricity generation of the CSP and PV and to model those variations as a set of linear equations too.

9 Concentrated Solar Power

In order to assess the energy potential of each days for the CSP, a 100 MW turbine nameplate capacity (also called power cycle's nameplate capacity in section 6.3.1) with a solar multiple of 1 designed for a direct irradiation of 950 W/m^2 was simulated at 2 operating conditions : a night only generation and an day only generation. For the night generation operating conditions, the CSP only used the energy collected from the solar irradiation to store thermal energy during daylight which is converted into electrical energy during the night. While during the only day generation, the energy collected from the solar field is directly converted into electrical energy without using the thermal storage. The objective is to simulate the relations between the power generated by the CSP when it uses thermal energy from the solar field and when it uses thermal energy from the TES.

SAM allows to choose the maximum turbine output at each hour of the simulation for each month. From the daily profile of the beam normal irradiation averaged over the entire year shown in Figure 10, the maximum turbine output was set at its maximum value from 8 p.m. to 6 a.m. and at 0 from 6 a.m. to 8 p.m such that the CSP would not generate electricity during the day for the night generation and at its maximum value from 6 a.m. and 0 from 8 p.m. to 6 a.m. without any thermal storage capacity for the day generation.

Finally, key results will be studied when the the nameplate capacity is changed (from 100 MW to 300 MW) and when the solar multiple is varied too (from SM = 1 to SM = 13).

9.1 Night generation

Figure 11 shows how the thermal energy charged in the thermal storage and the power sent to grid evolved during night generation. The power sent to grid is the net output power from the CSP taking into account the generation of the turbine and the multiple losses due especially to the work of pumps used to move the different fluids present in the CSP and heaters use to keep the HTF and the thermal storage fluid (TSF) over a certain temperature.

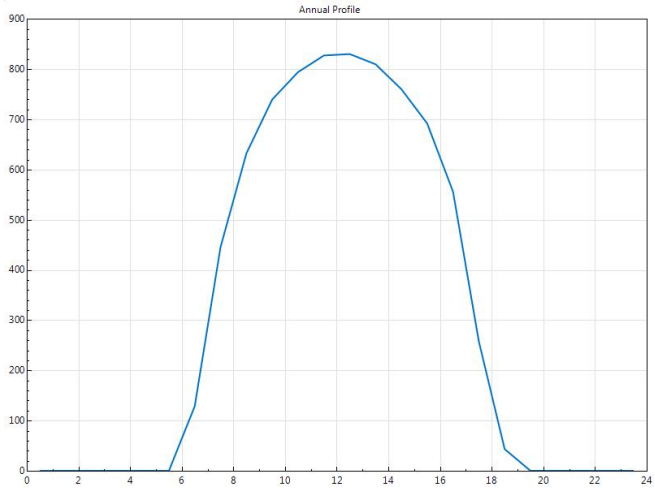

Figure 10: Daily profile of the beam normal irradiance averaged over the entire year in W/m^2 [13]

A 9 hours thermal storage capacity which, using Equation (19), is equivalent to 2806.18 MWht of energy capacity is used. The thermal storage is emptied every night to assure that the energy produced during the night is only from the energy stored the same day. To be sure that the maximum energy potential of each days is correctly assessed, it is important to check that the energy stored is never limited by the maximum thermal energy capacity of the CSP. Figure 12 shows the evolution of the TES charge state of the CSP trough the year generated by SAM. Since the energy stored presented in Figure 12 never exceed 2806.18 MWht, the values given by SAM are not capped by the maximum thermal energy capacity.

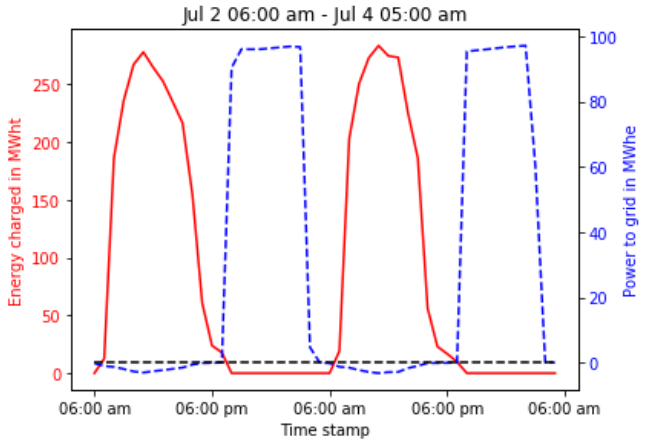

Figure 11: Evolution of the thermal energy charged and the electric power sent to grid from the 2^{nd} of July to the 4^{th} of July for the night generation

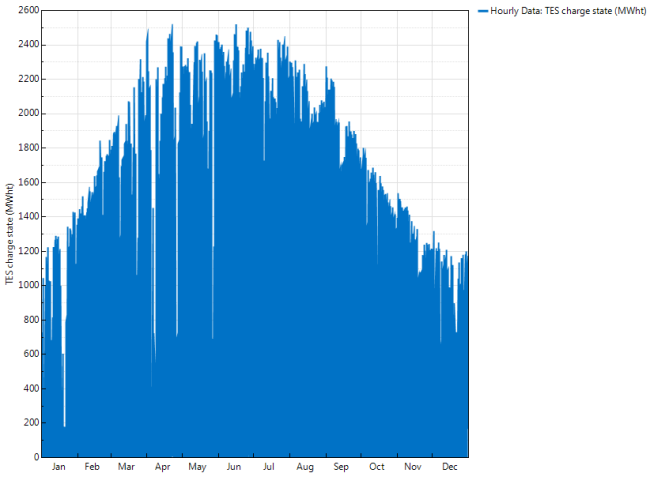

Figure 12: Evolution of the TES charge state of the CSP for the entire year for $SM = 1$, a 9 hours thermal energy storage at design point and a 100 MW turbine nameplate capacity [13]

9.1.1 Thermal energy leaving in HTF and relation with solar irradiation

The thermal energy leaving in HTF is the thermal energy transferred from the solar field to the other part parts of the CSP, either the power block or the thermal storage once the HTF has been heated enough by solar irradiation. Figure 13 shows its evolution as thermal power (but since it is an hourly generation, it is the total amount of power during 1 hour, it will be referred as energy) during the entire year.

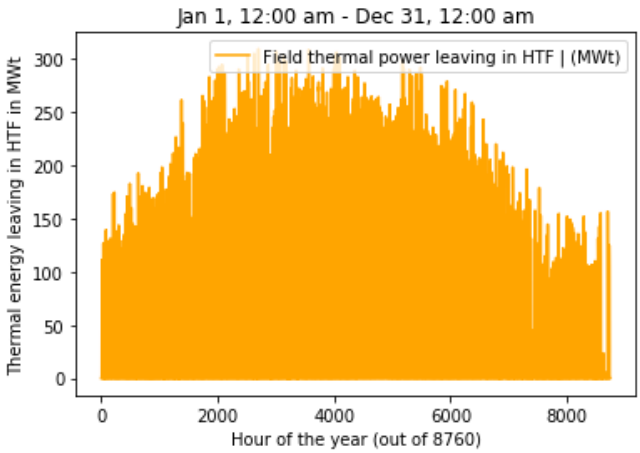

Figure 13: Evolution of the thermal power leaving in HTF for the entire year

As can been seen in Figure 13, the field thermal energy leaving in HTF is greater from approximately the 2000^{th} hour of the year to the 6000^{th} hour of the year than for the rest of the year. However, the direct irradiance seems to reach roughly the same values through the entire year as seen in Figure 14.

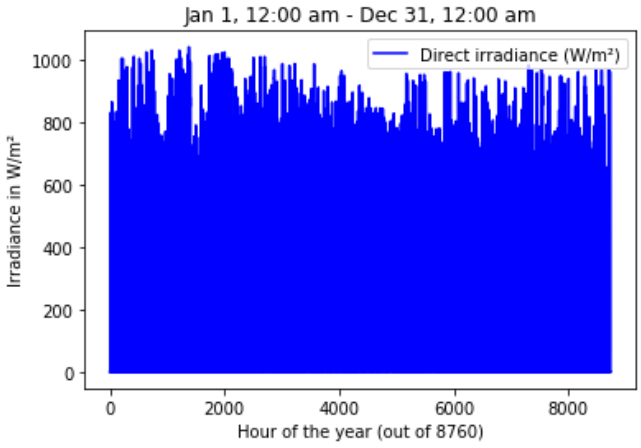

Figure 14: Evolution of the direct irradiance in Kôm Ombo for the entire year

This results can be explained be the thermal inertia of the HTF. Despite the fact that maximum values of direct irradiance do not seem to change that much over the entire year, or at least, not in a seasonal way such as the thermal energy leaving in HTF, the daylight duration does change and has a big impact on the thermal energy leaving in HTF. As can been in seen in graphs of Figure 15, when the direct irradiation does not last for a sufficient amount of time at a significant value (more than 200 W/m^2), less (and sometimes no) thermal energy are transferred from the HTF. This phenomena is due to the fact the HTF is not heated at a temperature enough high to be able to transfer thermal energy to the TSF, as seen in Figure 16.

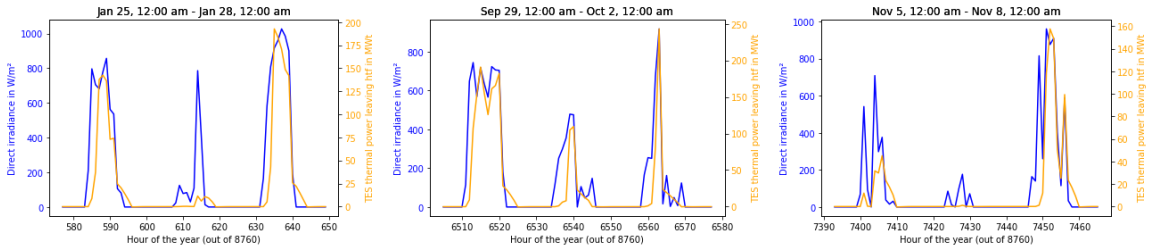

Figure 15: Evolution of the thermal energy leaving in htf with the direct solar irradiation at 3 different times of the year : from January 25^{th} to January 28^{th}, from September 29^{th} to October 2^{nd} and from November 5^{th} to November 8^{th}

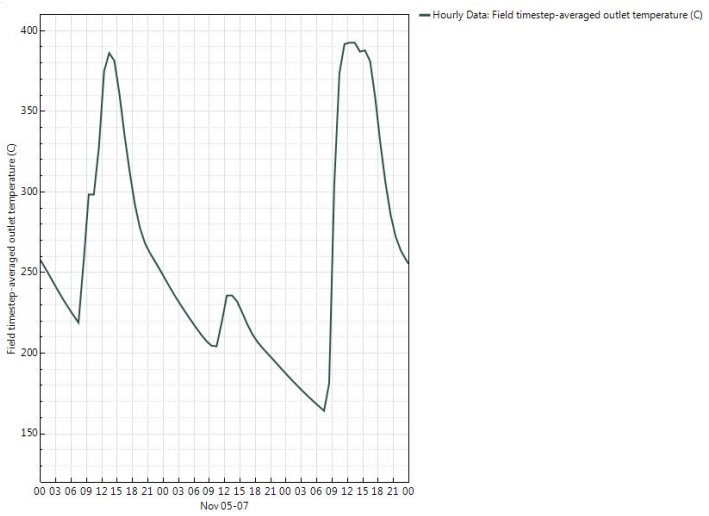

Figure 16: Evolution of the solar field outlet temperature from November 5^{th} to November 8^{th} [13]

9.1.2 Relation between energy leaving in HTF and energy charged in the thermal storage

Since during the night generation, the thermal energy collected by the solar field is only used to charge the thermal storage, the energy charged in the thermal storage should be the same than the thermal

energy leaving in HTF. Figure 17 shows that it is the most of the time the case.

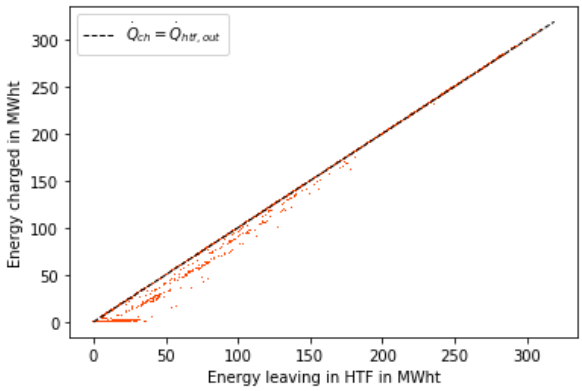

Figure 17: Evolution of the thermal energy charged in TES with respect to the thermal energy leaving in htf at the same hour

However, as can be seen in Figure 17, there are some values for which the thermal energy charged is lower than the thermal energy leaving in HTF. And this phenomenon becomes more prominent as the thermal energy leaving in HTF decreases. Graphs in Figure 18 show that this phenomenon takes place at the beginning of the charge of thermal energy when a part of the energy leaving in HTF is lost in parasitic losses.

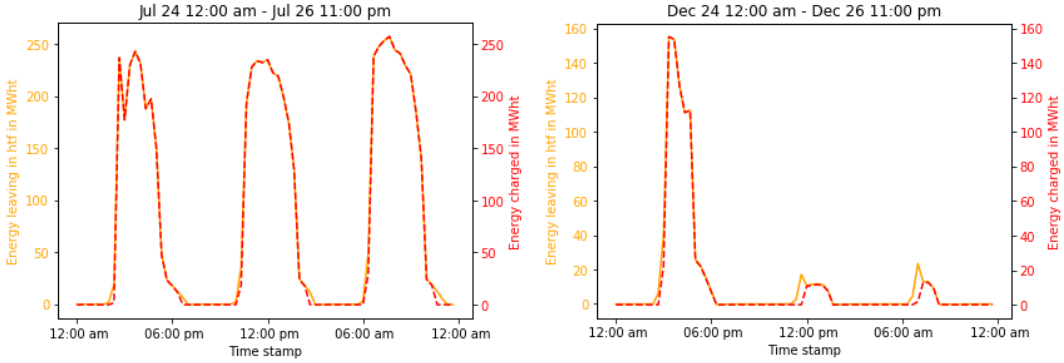

Figure 18: Evolution of the thermal energy charged in TES with the thermal energy leaving in HTF from July 24^{th} to July 26^{th} and from December 24^{th} to December 26^{th}

9.1.3 Relation between energy discharged from TES and power sent to grid during the night

One of the key relations that needs to be modeled is the relation between the energy discharged from the thermal storage and the power sent to grid. Since the CSP only generates during night, only the energy discharged from the storage is converted into electric power. Graphs in Figure 19 illustrate the

relations between the evolution of both results.

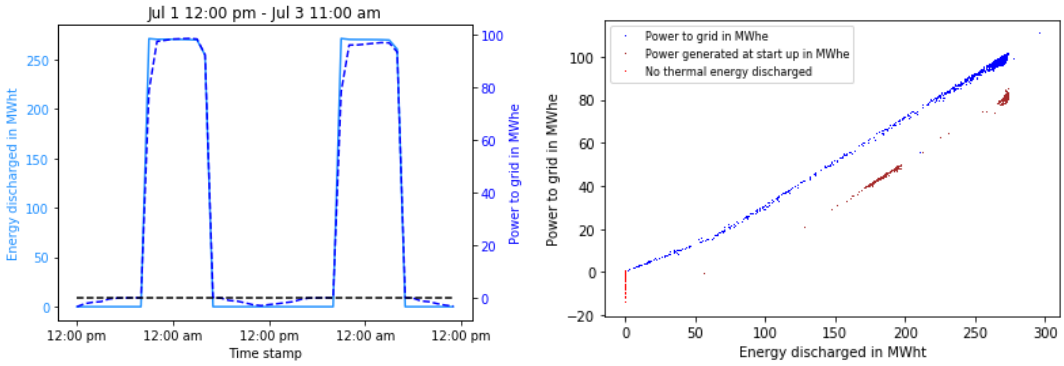

Figure 19: Evolution of the hourly values of the thermal energy discharged from the storage of the CSP and the electric power sent to grid from July 1^{st} to July 3^{rd} (on the left) and evolution of the power sent to grid with respect to the energy discharged at the same hour (on the right)

As can be seen in the graph on the left of Figure 19, the curve of the power sent to grid follows the curve of the energy discharged almost every hour as long as it is nighttime (from 8 p.m. to 6 a.m.). There is only a slight difference for the first hour of discharged of each day. This difference is due to the fact the fraction of thermal power needed for startup of the power cycle was fixed at 0.2 and the power block startup time at 0.5 hours. Therefore, as can be seen in the graph on the right of Figure 19, the thermal energy discharged is bigger than the power sent to grid at startup (in brown on the graph) compared to the values when the turbine has already been started (in blue on the graph). If the fraction of thermal power needed for startup and the power block startup time are reduced to 0, this difference in the first hour between the curve of the thermal energy discharged and the curve of the power sent to grid almost disappears as can be seen in graphs of Figure 20.

Since the goal of this section is to implement a model composed of linear equations, results from the simulation where the fraction of thermal power needed for startup and the power block startup time are fixed to 0 will be used. In those conditions, the relation between the thermal energy discharged and the power sent to grid can be approximated using a piece-wise linear regression as seen in Figure 21.

The piece-wise linear regression is defined in Equations (24) and (25) where $\dot{W}_{grid}$ is the electric power sent to grid and the $\dot{Q}_{th,disch}$ is the thermal energy discharged.

If $\dot{W}_{grid} \leq 20$ MWhe

$$\dot{W}_{grid} = 0.254 \cdot \dot{Q}_{th,disch} + 0.025 \tag{24}$$

If $\dot{W}_{grid} > 20$ MWhe

$$\dot{W}_{grid} = 0.398 \cdot \dot{Q}_{th,disch} - 8.456 \tag{25}$$

Over the entire year, the total amount of electric power sent to grid is 167.99 GWhe while using the piece-wise linear regression, the total amount is 167.879 GWhe which is a difference of only 0.066%.

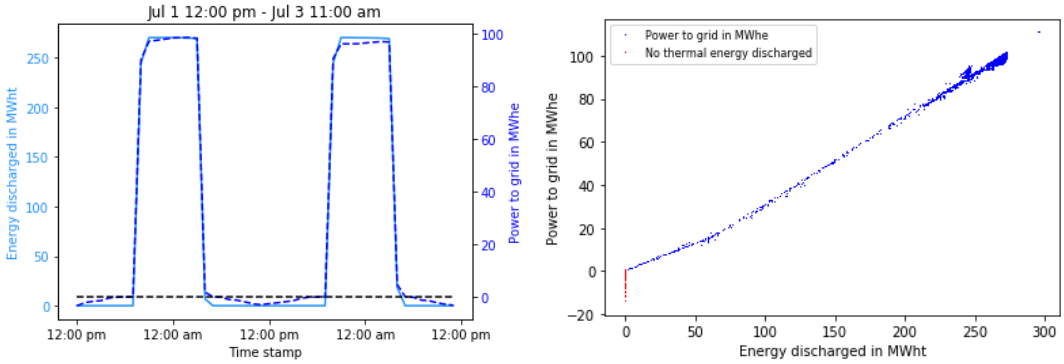

Figure 20: Evolution of the thermal energy discharged from the storage of the CSP with the power sent to grid from July 1^{st} to July 3^{rd} (on the left) and evolution of the power sent to grid with respect to the energy discharged at the same hour (on the right) when the power block startup time and the fraction of thermal power needed for startup are fixed to 0

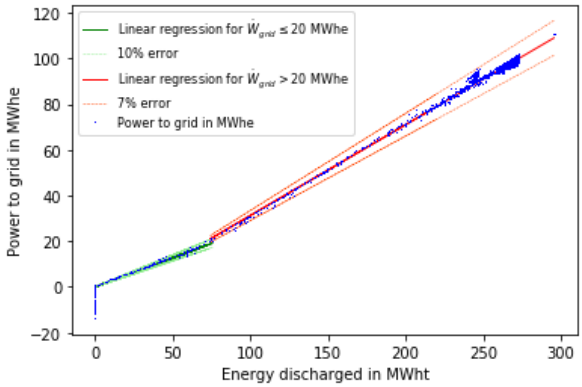

Figure 21: Evolution of the electric power sent to grid with respect to the thermal energy discharged at the same hour when the power block startup time and the fraction of thermal power needed for startup are fixed to 0 with its approximation using a piece-wise linear regression

9.1.4 Power consumed during the day

As can be seen in graphs of Figure 22, when the CSP is charging the thermal storage during the day, the power sent to grid is negative, hence, electric power is consumed by the CSP. There are 2 main reasons for power consumption during day. Most of the time, as in the left graph of Figure 22 and confirmed in Figure 23, the HTF pumping power, the power used by the pumps to move the HTF, is the major cause of losses during daytime.

Moreover, when the thermal storage has not been charged for a long time, temperature of the fluid within the hot tank could fall below the tank minimum temperature. In order to avoid it, heaters are used and are also a source of consumption during the day as seen in Figure 24.

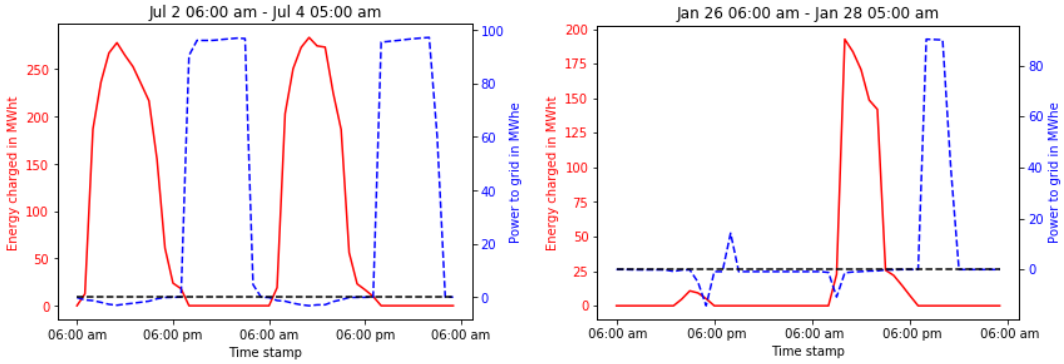

Figure 22: Evolution of the thermal energy charged with the electric power sent to grid from July 2^{nd} to July 4^{th} (on the left) and from January 26^{th} to January 28^{th} (on the right)

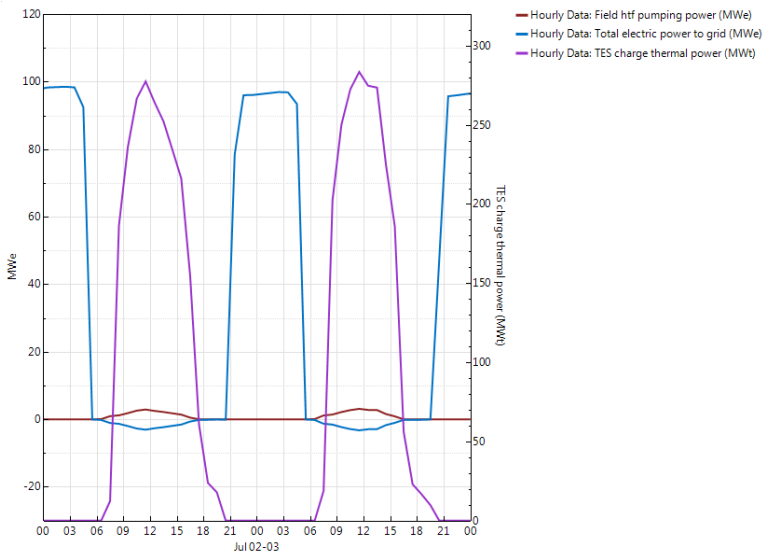

Figure 23: Evolution of the thermal energy charged with the electric power sent to grid and the field htf pumping power from July 2^{nd} to July 4^{th} [13]

In order to ease the modelling of both sources of consumption, the total daytime consumption was evaluated by summing the power sent to grid of each day from 6 a.m to 7 p.m. included. Then, its mean value will be used as the constant consumption of the CSP during daytime. The mean value is calculated by dividing the total daytime consumption by the number of hours of consumption. The total daytime consumption equals 4185.099 MW and its mean value equals 0.819 MW.

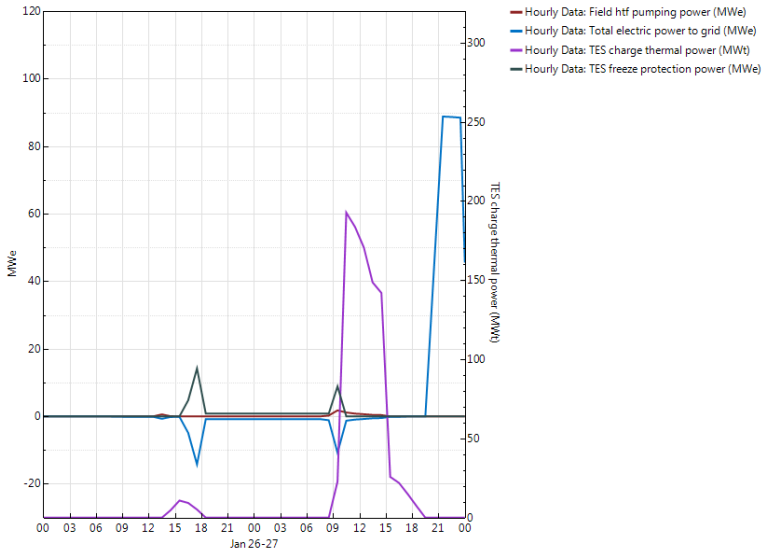

Figure 24: Evolution of the thermal energy charged with the electric power sent to grid, the field htf pumping power and the TES freeze protection power from January 26^{th} to January 28^{th} [13]

9.2 Day generation

The objective of the day generation is to model how the energy collected by the solar field is converted directly into electricity without being stored in the TES. To be sure that the entirety of the energy collected by the solar is converted into electricity, no thermal storage was added for this simulation.

9.2.1 Relation between the thermal energy leaving from HTF and the electric power sent to grid

Figure 25 shows the evolution of the electric power sent to grid with respect to the thermal energy leaving in HTF. From this figure, it can be seen that the thermal energy leaving in HTF begins to be converted only above a threshold value.

This observation is also seen on graphs in Figure 26 where the curve on the power sent to grid follows almost perfectly the curve of thermal energy leaving in HTF. However, the thermal energy is not converted into electric power for small values (below 40 MWht) since it does not bring enough heat to the power cycle produce steam.

Therefore, the power sent to grid can be approximated using a linear regression for values of the thermal energy leaving in HTF higher than 40 MWht. Figure 27 shows the linear regression and its mathematical expression is presented in Equation (26) where $\dot{W}_{grid,day}$ is the power sent to grid during daytime and $\dot{Q}_{htf,out}$ is the thermal energy leaving from HTF.

If $\dot{Q}_{htf,out} > 40$ MWht,

$$\dot{W}_{grid,day} = 0.393 \cdot \dot{Q}_{htf,out} - 9.779 \tag{26}$$

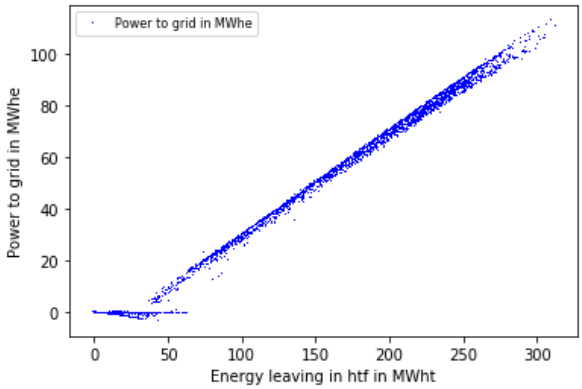

Figure 25: Evolution of the electric power sent to grid with respect to the thermal energy leaving in HTF during day generation

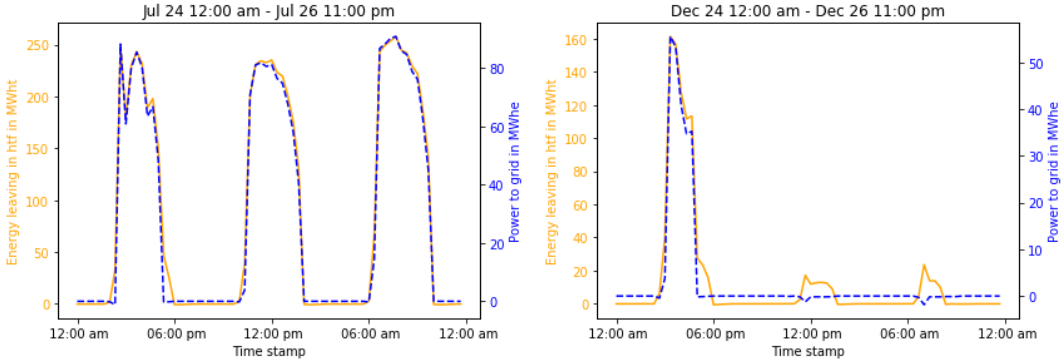

Figure 26: Evolution of the thermal energy leaving from HTF and the power sent to grid from July 24^{th} to July 26^{th} on the left and from December 24^{th} to December 26^{th} on the right

9.2.2 Power consumed during the night

As for the power consumed during night when there is no TES and no electricity generation during night, it is almost non-existent. Indeed, when summing the total amount of power sent to grid from 8 p.m. to 5 a.m. included, a total amount of 7.47 MWe of electric power is consumed for the entire year. Dividing this number by the number of hours of nighttime, only 0.002 MWe are consumed every hour on average during night. This consumption is solely due to the field HTF pumping power that move the HTF at the minimum mass flow during night.

9.3 Study of the turbine nameplate capacity

The previous simulations were done with a 100 MW turbine nameplate capacity. However, nameplate capacity up to 300 MW can be used for utility-scale project. In order to provide the opportunity to determine the best turbine nameplate capacity for the CSP in the optimization problem, the impact

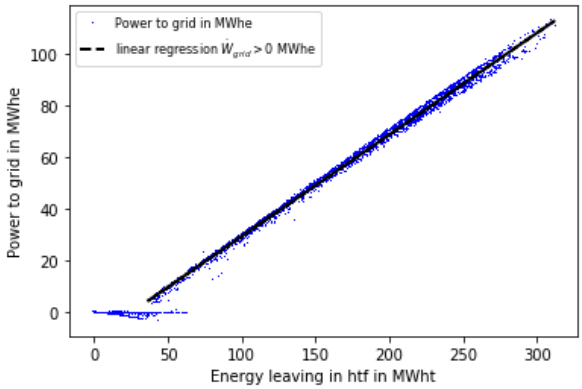

Figure 27: Evolution of the thermal energy charged in TES relative to the thermal energy leaving in HTF

of the nameplate capacity was studied for the relations defined earlier. The study was done at the same operating conditions than for the night generation and day generation except that the turbine nameplate capacity was varied from 100 MW to 300 MW by a step of 50 MW.

9.3.1 Thermal energy leaving in HTF

In order to study the evolution of the thermal energy leaving in HTF, its mean value was assessed for the different nameplate capacities. Those mean values were assessed by dividing the total amount of energy leaving in HTF over the entire year by the number of hour during daytime. Figure 28 shows the evolution of the mean value of the thermal energy leaving in HTF with respect to the turbine nameplate capacity during night generation operating conditions.

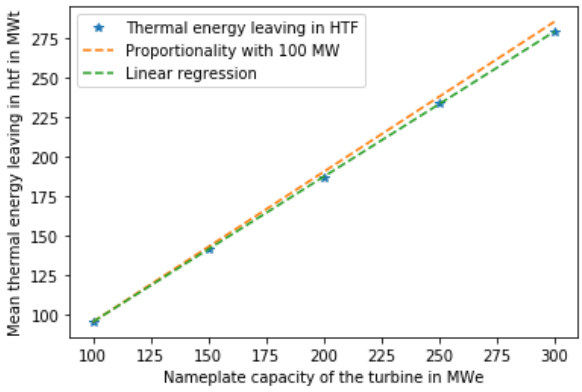

Figure 28: Evolution of the mean of thermal energy leaving in HTF with respect to the nameplate capacity of the turbine during night generation

As can be seen in Figure 28, the most accurate way to approximate the evolution is to use a linear

regression. Equation (27) gives the expression of the linear regression where $\dot{Q}_{htf,out,mean}$ is the mean value of the thermal energy leaving in HTF and W_{turb} is the nameplate capacity of the turbine.

$$\dot{Q}_{htf,out,mean} = 0.919 \cdot W_{turb} + 3.182 \tag{27}$$

The maximum hourly values of the thermal energy leaving in HTF can be approximated using a rule of 3 as described in Equation (28). In this equation, the ratio between the mean value of the thermal energy for the nameplate capacity W_{turb} and a nameplate capacity of 100 MW is considered to be equal with the ratio between any value of the thermal energy at W_{turb} and the value of thermal energy for a 100 MW capacity for the same hour.

$$\frac{\dot{Q}_{htf,out,mean,W_{turb}}}{\dot{Q}_{htf,out,mean,100MW}} = \frac{\dot{Q}_{htf,out,W_{turb}}}{\dot{Q}_{htf,out,100MW}} \tag{28}$$

$\dot{Q}_{htf,out,mean,W_{turb}}$ is the mean value of the thermal energy leaving in HTF for a turbine nameplate capacity of W_{turb}, $\dot{Q}_{htf,out,mean,100MW}$ is the mean value of the thermal energy leaving in HTF for a turbine nameplate capacity of 100 MW, $\dot{Q}_{htf,out,W_{turb}}$ is the value of the thermal energy leaving in HTF at a certain hour of the year for a turbine nameplate capacity of W_{turb} and $\dot{Q}_{htf,out,100MW}$ the value of the thermal energy leaving in HTF at a certain hour of the year for a nameplate capacity of 100 MW. By developing Equation (28), the relation between the thermal energy leaving in HTF at any hour of the day for any W_{turb} and the thermal energy leaving in HTF for a nameplate capacity of 100 MW can be described as seen in Equations (29) and (30).

$$\dot{Q}_{htf,out,W_{turb}} = \frac{\dot{Q}_{htf,out,mean,W_{turb}}}{\dot{Q}_{htf,out,mean,100MW}} \cdot \dot{Q}_{htf,out,100MW} \tag{29}$$

$$\iff \dot{Q}_{htf,out,W_{turb}} = \frac{0.919 \cdot W_{turb} + 3.182}{0.919 \cdot 100 + 3.182} \cdot \dot{Q}_{htf,out,100MW} \tag{30}$$

9.3.2 Thermal energy charged in the TES

Similarly to the thermal energy leaving in HTF, the mean values of the thermal energy charged in the TES were used to study the evolution of the nameplate capacity. Figure 29 shows the evolution of the mean value of the thermal energy charged in TES with respect of the turbine nameplate capacity during night generation.

As with the thermal energy leaving in HTF, the most accurate way to approximate the evolution is to use a linear regression. Its expression is given in Equation (31).

$$\dot{Q}_{ch,mean} = 0.902 \cdot W_{turb} + 3.338 \tag{31}$$

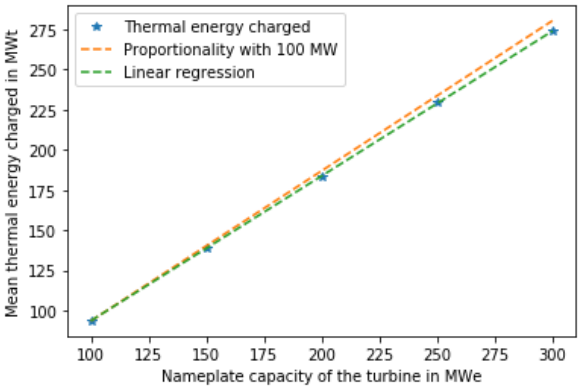

Figure 29: Evolution of the mean of thermal energy charged in TES with respect to the nameplate capacity of the turbine during night generation

Using the same development than for thermal energy leaving in HTF, the maximum hourly values of the thermal energy charged in TES can be approximated using a rule 3 as in Equations (32), (33), (34).

$$\frac{\dot{Q}_{ch,mean,W_{turb}}}{\dot{Q}_{ch,mean,100MW}} = \frac{\dot{Q}_{ch,W_{turb}}}{\dot{Q}_{ch,100MW}} \tag{32}$$

$$\iff \dot{Q}_{ch,W_{turb}} = \frac{\dot{Q}_{ch,mean,W_{turb}}}{\dot{Q}_{ch,mean,100MW}} \cdot \dot{Q}_{ch,100MW} \tag{33}$$

$$\iff \dot{Q}_{ch,W_{turb}} = \frac{0.902 \cdot W_{turb} + 3.338}{0.902 \cdot 100 + 3.338} \cdot \dot{Q}_{ch,100MW} \tag{34}$$

$\dot{Q}_{ch,mean,W_{turb}}$ is the mean value of the thermal energy charged in TES for a turbine nameplate capacity of W_{turb}, $\dot{Q}_{ch,mean,100MW}$ is the mean value of the thermal energy charged in TES for a turbine nameplate capacity of 100 MW, $\dot{Q}_{ch,W_{turb}}$ is the value of the thermal energy charged in TES at a certain hour of the year for a turbine nameplate capacity of W_{turb} and $\dot{Q}_{ch,100MW}$ the value of the thermal energy charged in TES at the same hour of the year for a nameplate capacity of 100 MW.

9.3.3 Power to grid from thermal energy discharged

In order to assess the evolution of the relation between the thermal energy discharged from TES and the power sent to grid, the slopes and the intercepts of Equations (24) and (25) were computed for each turbine nameplate capacity. The piece-wise linear regression was made for values of the power sent to grid below 20% of the turbine nameplate capacity and for values of the power sent to grid above 20% of the nameplate capacity. Their evolution are shown on graphs of Figure 30.

As can be seen on the left graph of Figure 30, the slopes of Equations (24) and (25) do not vary much. Therefore, the mean of their values was used to approximate the slopes for all size of nameplate capacity (0.254 for values below 20% of the nameplate capacity and 0.398 for values above). As for the

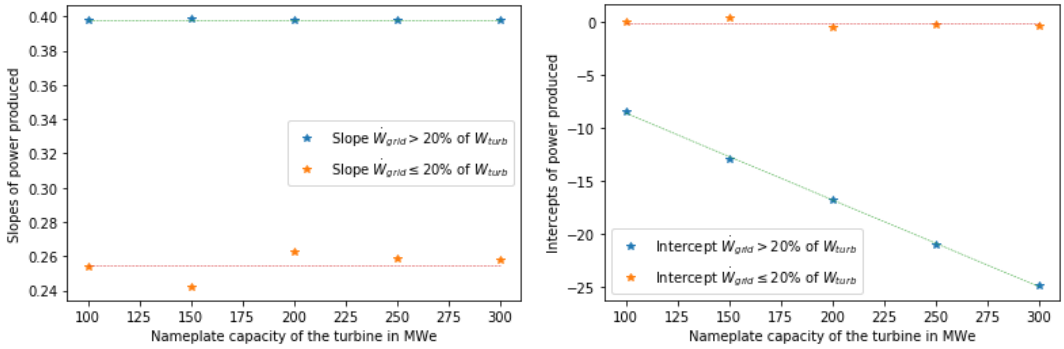

Figure 30: Evolution of the slopes of Equations (24) and (25) with respect to the nameplate capacity of the turbine (graph on the left) and evolution of the intercepts of Equations (24) and (25) with respect to the nameplate capacity of the turbine (graph on the right)

intercepts, for values of the power sent to grid below 20% of nameplate capacity, they remain around 0 and for values above 20% of the nameplate capacity, a linear regression was used to approximate its evolution. Equations (35) and (36) show the expressions of the relation between the power sent to grid and the energy discharged for all size of nameplate capacity.

If $\dot{W}_{grid} \leq 20\ \%\ W_{turb}$

$$\dot{W}_{grid} = 0.254 \cdot \dot{Q}_{th,disch} \tag{35}$$

If $\dot{W}_{grid} > 20\ \%\ W_{turb}$

$$\dot{W}_{grid} = 0.398 \cdot \dot{Q}_{th,disch} + (-0.414 - 0.082 \cdot W_{turb}) \tag{36}$$

9.3.4 Power to grid from thermal energy leaving in htf

Similarly to the power sent to grid from thermal energy discharged from TES, the evolution of the power sent to grid from the thermal energy leaving in HTF was evaluated by computing the slope and the intercept of Equation (26). Their evolution are shown on graphs in Figure 31.

As can be seen in Figure 31, the evolution of slope and the intercept can be approximated using a linear regression expressed in Equations (37) and (38). Moreover, as for Equation (26), a minimal value of thermal energy leaving in HTF must be collected in order to start the generation of electricity by the turbine. For each nameplate capacity, the minimal value of thermal energy leaving in HTF is given in Table 17 in percentage of the cycle thermal power at design. From the nameplate capacity, the cycle thermal power at design noted $\dot{Q}_{th,pc}$ is given in Equation (39).

$$Slope_{\dot{W}_{grid}} = -0.000026 \cdot W_{turb} + 0.395 \tag{37}$$

$$Intercept_{\dot{W}_{grid}} = -0.089 \cdot W_{turb} - 0.916 \tag{38}$$

$$\dot{Q}_{th,pc} = \frac{W_{turb}}{\eta_{pc,gtn} \cdot \eta_{pc,th}} \tag{39}$$

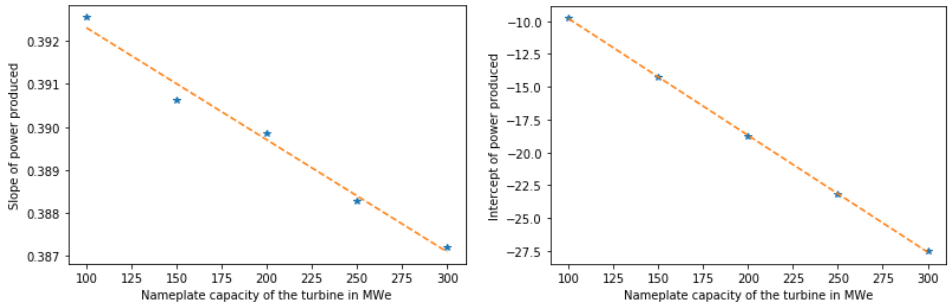

Figure 31: Evolution of the slope of Equation (26) with respect to the turbine nameplate capacity (graph on the left) and evolution of the intercept of Equation (26) with respect to the turbine nameplate capacity(graph on the right)

$\eta_{pc,gtn}$ is the estimated gross to net conversion factor of the turbine and $\eta_{pc,th}$ is the cycle thermal efficiency. Their values were given in Table 8.

Turbine nameplate capacity in MWe	**Minimum thermal energy leaving in HTF required in MWht**	**Cycle thermal power at design $\dot{Q}_{th,pc}$ in MWt**	**Minimum thermal energy leaving in HTF required as percentage of the $\dot{Q}_{th,pc}$**
100	40	312.11	12.82 %
150	57	468.16	12.17 %
200	80	624.22	12.82 %
250	100	780.27	12.82 %
300	111	936.33	11.52 %

Table 17: Minimum thermal energy leaving in HTF required to be directly converted into electric power in MWht and as percentage of the cycle thermal power at design

From Equations (37) and (38), the relation between the power sent to grid and the thermal energy leaving in HTF is given in Equation (40).

$$\dot{W}_{grid,day} = (-0.000026 \cdot W_{turb} + 0.395) \cdot \dot{Q}_{htf,out} + (-0.089 \cdot W_{turb} - 0.916) \tag{40}$$

9.3.5 Power consumed during the day and the night

Like for the thermal energy leaving in HTF and thermal energy charged in TES, the evolution of the power consumed during day and during night were evaluated using their mean values for each turbine nameplate capacity. The graphs in Figure 32 show their evolution.

Those values can be approximated by a linear regression. The expressions of the average power consumed during day and during night with respect to the turbine nameplate capacity are given in

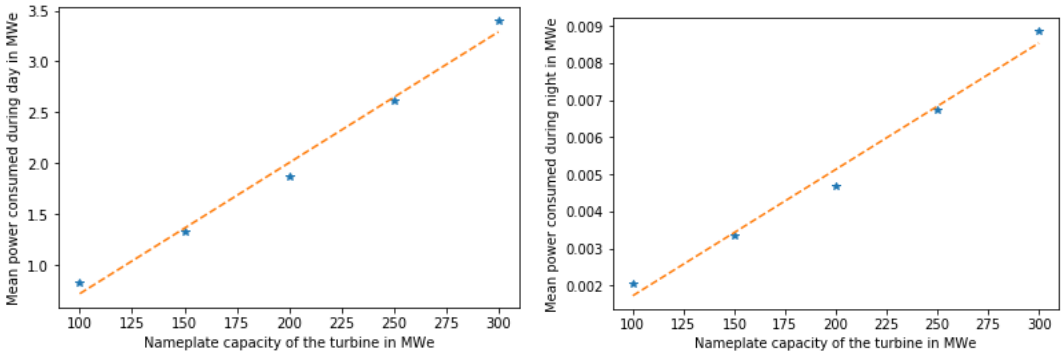

Figure 32: Evolution of the mean of the power consumed during day (on the left graph) and the power consumed during night (on the right graph) with respect to the nameplate capacity of the turbine

Equations (41) and (42).

$$\dot{W}_{cons,day,hour} = -0.569 + 0.013 \cdot W_{turb} \tag{41}$$

$$\dot{W}_{cons,night,hour} = 0.000034 \cdot W_{turb} - 0.0017 \tag{42}$$

9.4 Impact of the solar multiple on thermal energy and power consumed

The other variable studied is the solar multiple SM. As a reminder, it is a measure of the solar field aperture area expressed as a multiple of the aperture area needed to operate the power cycle at its design capacity. For $SM = 1$, if the solar field is hit by a solar direct normal irradiation at design point (950 W/m^2 here), the thermal power collected will be able to run the turbine of the power cycle at its nominal capacity. Therefore, in order to be able to run the turbine at its nominal value while charging the TES, SM is usually bigger than 1.

This section will evaluate how the thermal energy collected by the solar and charged in the TES are affected by the increase of SM. Moreover, since one of the main sources of losses are the pumping power of the solar field, the effect on power consumed during day and night will be assessed too. The results will be expressed in term of ratio between the total amount of thermal energy or the total amount of power consumed at a certain SM during a chosen period and the total amount of thermal energy or the total amount of power consumed for $SM = 1$ during the same chosen period. The objective is to approximate the effect of the solar multiple knowing the hourly values for the maximum thermal energy and the power consumed for $SM = 1$.

Moreover, as stated earlier, the ratio will be computed during a chosen period. During the previous simulations for the night generation, for $SM = 1$ and a 9 hours thermal storage capacity, the thermal storage is never fully charged. Therefore, the thermal energy collected by the solar field and charged in the TES are not capped by the TES capacity and are always at their maximum hourly values. Nevertheless, when the solar multiple is increased, the thermal energy leaving in HTF is increased such that a 9 hours thermal storage might not be enough to avoid the capping of the thermal energy collected and charged as can be seen in Figure 33 for $SM = 2$.

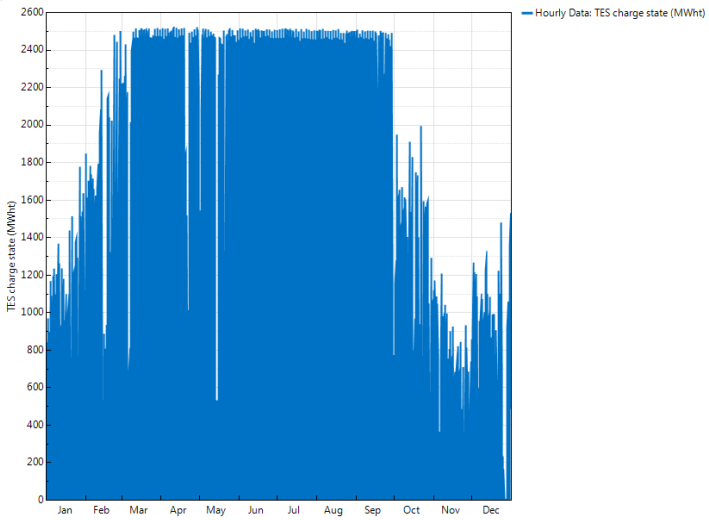

Figure 33: Evolution of the TES charge state of the CSP for the entire year for $SM = 2$, a 9 hours thermal energy storage at design point and a 100 MW turbine nameplate capacity [13]

To take that into account, the time of hours storage is increased for simulations where the SM is bigger than 1. Furthermore, the ratio will be computed for the period during which the maximum capacity of the TES is not reached yet. Table 18 shows the hours of thermal storage chosen for each SM and the period (number of hours from the 1^{st} hour of the year) for which the ratio is computed.

Solar multiple	**Hours of thermal storage at design**	**Periods before the maximum of TES is reached**
1	9	8760
2	18	1880
3	27	1452
4	100	1488
5	100	888
6	100	648
7	200	792
8	200	672
9	200	504
10	200	408
11	200	312
12	200	264
13	200	216

Table 18: Hours of thermal storage at design point and periods before maximum TES is reached for each solar multiple for which the ratios of thermal energy and power consumed will be computed

Despite the small number of periods for the highest solar multiple, the hours of thermal storage at design was not set above 200 hours. The reason lies in the fact that for hours above 200 hours, the temperature of the hot tanks fall below its minimum temperature before being completely charged. The heater is therefore constantly used and affects greatly the power produced and consumed.

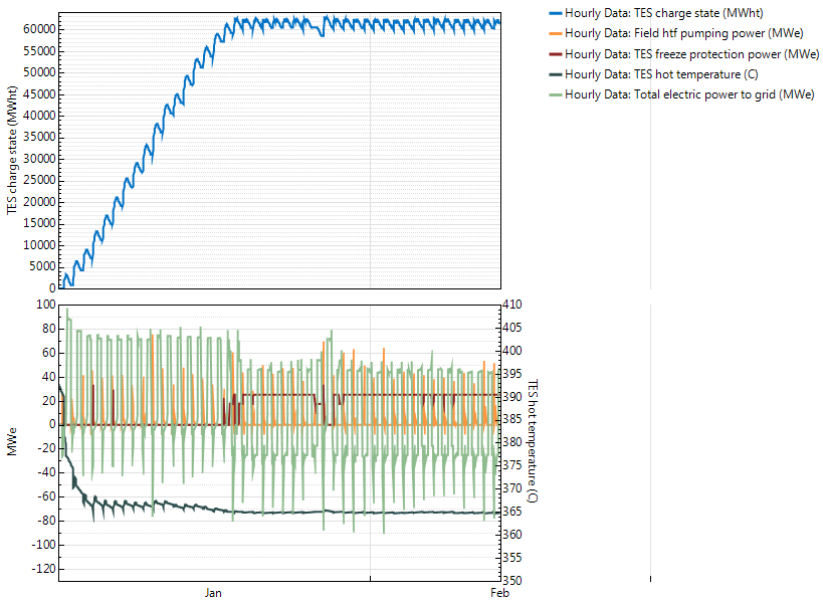

Figure 34: Evolution of the TES charge state of the CSP, the field HTF pumping power, the TES freeze protection power, the TES hot temperature and the electric power sent to grid for $SM = 13$, a 300 hours thermal energy storage at design point and a 100 MW turbine nameplate capacity from January 1^{st} to mid February [13]

For instance, in Figure 34, the freeze protection power is almost constantly used from mid January slightly before the TES reaches its maximum capacity for a 300 hours thermal energy storage. It is due to the fact that the energy brought from the solar field is not enough to heat the hot tank significantly when it is almost full. However, tanks are not that large in reality, therefore, this phenomenon is not taking into account in the computation of the ratio.

9.4.1 Power consumed during the day

The first thing to determine in order to approximate the power consumed with respect to the solar multiple is the optimal number of field subsections for each solar multiple. As a reminder, the number of field subsection defines the location and the shape of the header piping as seen in Figure 8. To be more accurate, it determines the diameter and the number of the runner pipes (the pipes connecting the solar field with the power block and the thermal storage) and header pipes (pipes connecting the field loops) and, therefore, impact the mass flow rate of the HTF and the power consumed by the pump. Figure 35 shows how the power sent to grid, and especially the power consumed varied with the number of field subsections for a solar multiple of 5.

As can be seen in Figure 35, the power consumed, shown as negative values of the power sent to grid, decreases as the number of field subsections increases. However, increasing the number of field subsection slightly increases the heat losses in the solar field too, therefore the energy charged decreases and less power can be generated from the TES. The number of field subsections must be

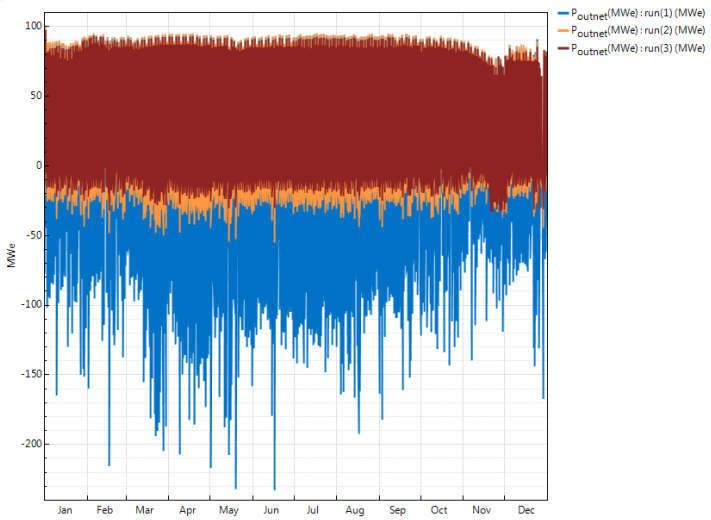

Figure 35: Evolution of the electric power sent to grid for $SM = 5$, a 100 MW nameplate capacity and a 100 hours TES at design point for different number of field subsections. The number of field subsections equals 1 for run(1) (in blue), 2 for run(2) (in orange) and 4 for run(3) (in brown) [13]

chosen such as it decreases sufficiently the power consumed without decreasing too much the thermal energy charged. The optimal numbers of field subsections for each solar multiple are shown in Table 19.

Solar multiple	**1**	**2**	**3**	**4**	**5**	**6**	**7**	**8**	**9**	**10**	**11**	**12**	**13**
Number of field subsections	2	2	4	4	4	6	6	6	6	6	6	10	8

Table 19: Number of field subsections for each solar multiple

Figure 36 shows the evolution of the ratio of power consumed for each solar multiple. In order to approximate those values, a piece-wise linear regression was used. Their expression are given in Equations (43), (44) and (45).

If $SM \leq 8$,

$$Ratio_{\dot{W}_{cons,day},SM} = SM \tag{43}$$

If $8 < SM \leq 10$,

$$Ratio_{\dot{W}_{cons,day},SM} = 3.776515 \cdot SM - 21.802248 \tag{44}$$

If $10 < SM \leq 13$,

$$Ratio_{\dot{W}_{cons,day},SM} = 1.942354 \cdot SM - 3.849975 \tag{45}$$

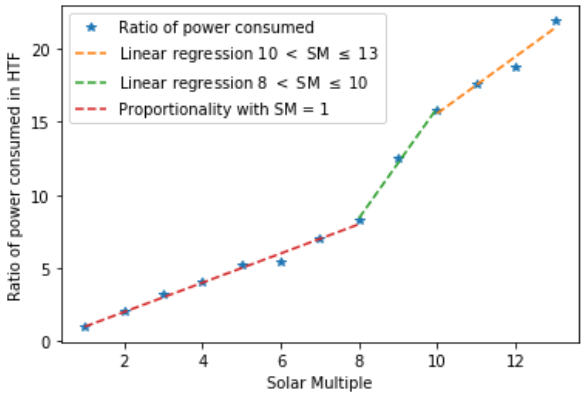

Figure 36: Evolution of the ratio of power consumed during day with respect to the solar multiple

9.4.2 Energy leaving in htf

The evolution of the ratio of the thermal energy leaving in HTF with respect to the solar multiple is shown in Figure 37. A linear regression can be used to approximate the values and its expression given in Equation (46)

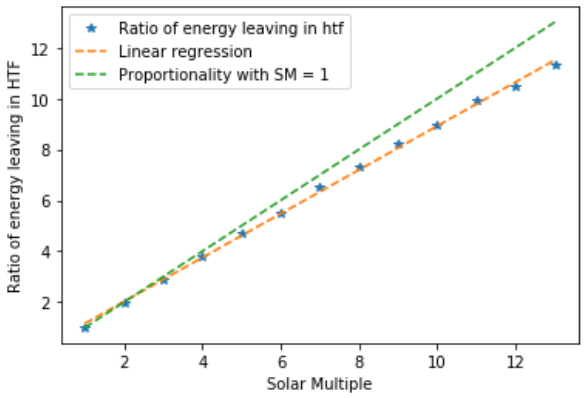

Figure 37: Evolution of the ratio of the thermal energy leaving in HTF with respect to the solar multiple

$$Ratio_{\dot{Q}_{htf},SM} = 0.862019 \cdot SM + 0.301699 \tag{46}$$

9.4.3 Energy charged in TES

The evolution of the ratio of the thermal energy leaving in HTF with respect to the solar multiple is shown in Figure 38. Similarly to the energy leaving in HTF, a linear regression can be used to approximate the values and its expression given in Equation (47).

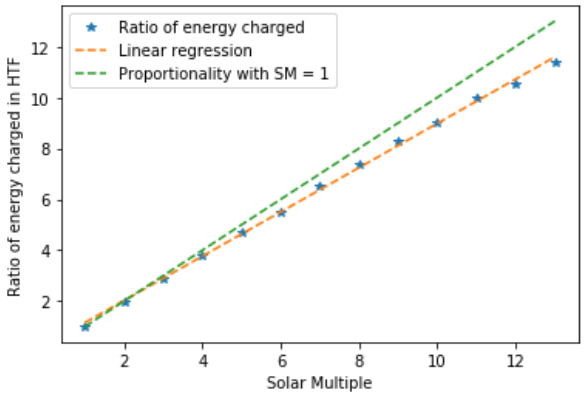

Figure 38: Evolution of the thermal energy charged in TES with respect to the solar multiple

$$Ratio_{\dot{Q}_{ch},SM} = 0.869464 \cdot SM + 0.288083 \tag{47}$$

9.4.4 Power consumed during the night

As for the power consumed during night, Figure 39 shows the evolution of the ratio of power consumed during day for each solar multiple. Their values were approximated using a piece-wise linear regression. Its expressions are given in Equations (48), (49) and (50). Simulations did not run above $SM = 11$ in SAM.

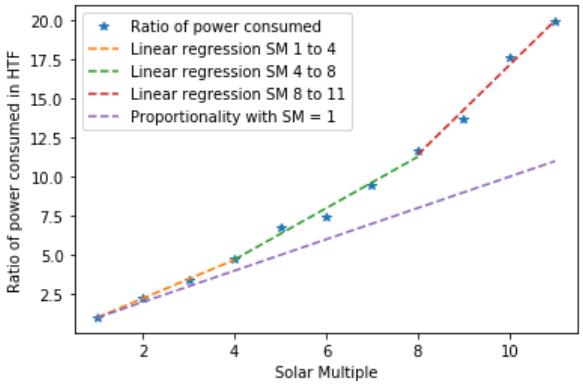

Figure 39: Evolution of the power consumed during night with respect of the solar multiple

If $1 \leq SM \leq 4$,

$$Ratio_{\dot{W}_{cons,night},SM} = 1.232490 \cdot SM - 0.229621 \tag{48}$$

If $4 < SM \leq 8$,

$$Ratio_{\dot{W}_{cons,night},SM} = 1.640239 \cdot SM - 1.851743 \tag{49}$$

If $8 < SM \leq 11$,

$$Ratio_{\dot{W}_{cons,night},SM} = 2.860630 \cdot SM - 11.486026 \tag{50}$$

9.5 Final equations

From the expressions determined earlier with the study of the effects of the nameplate capacity of the turbine and the solar multiple, this subsection presents the final expressions that will be used to simulate the thermal energy and power produced and consumed in the optimization problem.

9.5.1 Thermal energy leaving in htf

Using the hourly values of the thermal energy leaving in HTF for a solar multiple of 1 and a turbine nameplate capacity of 100 MW noted $\dot{Q}_{htf,out,100MW}$, the hourly thermal energy leaving in HTF can be simulated for a solar multiple of value SM and nameplate capacity W_{turb} from Equation (51).

$$\dot{Q}_{htf,out,W_{turb},SM} \leq Ratio_{\dot{Q}_{htf},SM} \cdot \dot{Q}_{htf,out,W_{turb}} \tag{51}$$

where

$$Ratio_{\dot{Q}_{htf},SM} = 0.862019 \cdot SM + 0.301699 \tag{52}$$

$$\dot{Q}_{htf,out,W_{turb}} = \frac{0.919 \cdot W_{turb} + 3.182}{0.919 \cdot 100 + 3.182} \cdot \dot{Q}_{htf,out,100MW} \tag{53}$$

Since $\dot{Q}_{htf,out,100MW}$ is the maximum thermal energy leaving in HTF for $SM = 1$ and $W_{turb} = 100$ MW, its approximation serves as ceiling values for the thermal energy leaving in HTF.

9.5.2 Thermal energy charged from solar field

Using the hourly values of the thermal energy charged from solar field for a solar multiple of 1 and a turbine nameplate capacity of 100 MW noted $\dot{Q}_{ch,100MW}$, the hourly thermal energy charged from the solar field can be simulated for a solar multiple of value SM and nameplate capacity W_{turb} from Equation (54).

$$\dot{Q}_{ch,W_{turb},SM} \leq Ratio_{\dot{Q}_{ch},SM} \cdot \dot{Q}_{ch,W_{turb}} \tag{54}$$

where

$$Ratio_{\dot{Q}_{ch},SM} = 0.869464 \cdot SM + 0.288083 \tag{55}$$

$$\dot{Q}_{ch,W_{turb}} = \frac{0.902 \cdot W_{turb} + 3.338}{0.902 \cdot 100 + 3.338} \cdot \dot{Q}_{ch,100MW} \tag{56}$$

Since $\dot{Q}_{ch,100MW}$ is the maximum thermal energy charged for $SM = 1$ and $W_{turb} = 100$ MW, its approximation serves as ceiling values for the thermal energy charged.

9.5.3 Power produced from the thermal storage

The hourly electric power sent to grid from the energy discharged from the thermal storage for a turbine nameplate capacity of W_{turb} can be simulated using Equations (57) and (58).

If $\dot{W}_{grid} \leq 20\ \%\ W_{turb}$

$$\dot{W}_{grid} = 0.254 \cdot \dot{Q}_{th,disch} \tag{57}$$

If $\dot{W}_{grid} > 20\ \%\ W_{turb}$

$$\dot{W}_{grid} = 0.398 \cdot \dot{Q}_{th,disch} + (-0.414 - 0.082 \cdot W_{turb}) \tag{58}$$

9.5.4 Power produced from the solar field

For the power produced from the solar field, a part of the thermal energy leaving in HTF might be used to charge the thermal storage. Therefore, the hourly thermal energy that will be directly converted into electricity noted $\dot{Q}_{htf,out,W_{grid}}$ is assumed to be the difference between the hourly thermal energy leaving in HTF and the hourly thermal energy charged. The hourly power produced from the solar field is given in Equation (59).

$$\dot{W}_{grid} = (-0.000026 \cdot W_{turb} + 0.395) \cdot \dot{Q}_{htf,out,W_{grid}} + (-0.089 \cdot W_{turb} - 0.916) \leq W_{turb} \tag{59}$$

where

$$\dot{Q}_{htf,out,W_{grid}} = \dot{Q}_{htf,out,W_{turb},SM} - \dot{Q}_{ch,W_{turb},SM} \tag{60}$$

9.5.5 Power consumed during the day

The hourly power consumed during day when no power is sent to the grid is simulated using Equation (61).

$$\dot{W}_{cons,day,W_{turb},SM} = Ratio_{\dot{W}_{cons,day},SM} \cdot \dot{W}_{cons,day,W_{turb}} \tag{61}$$

where

$$\dot{W}_{cons,day,W_{turb}} = -0.569 + 0.013 \cdot W_{turb} \tag{62}$$

If $SM \leq 8$,

$$Ratio_{\dot{W}_{cons,day},SM} = SM \tag{63}$$

If $8 < SM \leq 10$,

$$Ratio_{\dot{W}_{cons,day},SM} = 3.776515 \cdot SM - 21.802248 \tag{64}$$

If $10 < SM \leq 13$,

$$Ratio_{\dot{W}_{cons,day},SM} = 1.942354 \cdot SM - 3.849975 \tag{65}$$

9.5.6 Power consumed during night

The hourly power consumed during night when no power is sent to the grid is simulated using Equation (66).

$$\dot{W}_{cons,night,W_{turb},SM} = Ratio_{\dot{W}_{cons,night,SM}} \cdot \dot{W}_{cons,night,W_{turb}} \tag{66}$$

where

$$\dot{W}_{cons,night,W_{turb}} = 0.000034 \cdot W_{turb} - 0.0017 \tag{67}$$

If $1 \leq SM \leq 4$,

$$Ratio_{\dot{W}_{cons,night,SM}} = 1.232490 \cdot SM - 0.229621 \tag{68}$$

If $4 < SM \leq 8$,

$$Ratio_{\dot{W}_{cons,night,SM}} = 1.640239 \cdot SM - 1.851743 \tag{69}$$

If $8 < SM \leq 11$,

$$Ratio_{\dot{W}_{cons,night,SM}} = 2.860630 \cdot SM - 11.486026 \tag{70}$$

10 PVs

In order to assess the electric power produced by the PV, a 1 GWdc system nameplate capacity was simulated using SAM. Figure 40 shows the evolution of the system power generated from the PV system along with the module temperature and the weather file ambient temperature.

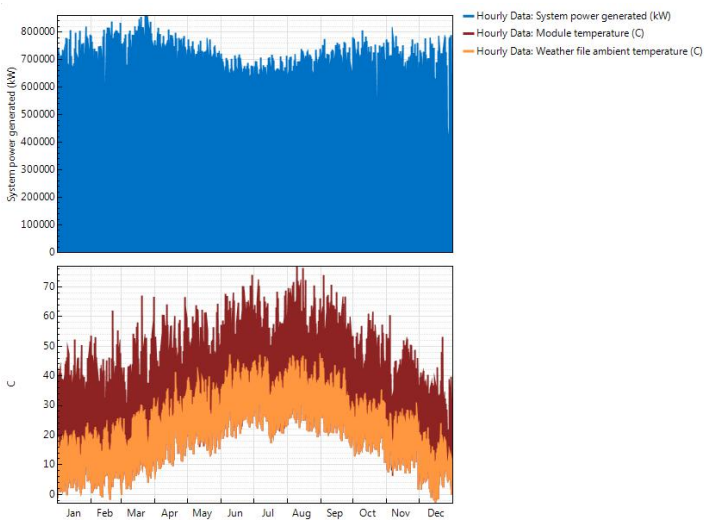

Figure 40: Evolution of the power produced by the 1 GWdc PV system (in blue), the module temperature (in brown) and the weather file ambient temperature (in orange) over the entire year of the simulation [13]

Unlike the CSP, the power generated from the PV reaches its highest values in the beginning and the end of the year (therefore in winter). Those results are mainly due to the impact of the ambient temperature on the PV cells. Indeed, as seen on the second graph of Figure 40, the ambient temperatures are at their highest values in summer. However, an increase in ambient temperature increases the module temperature which decreases the performance of the PV cells.

Furthermore, since the PV system converts photons from the diffuse irradiance and the global horizontal irradiance along with the photons from direct irradiance, it is not impacted as much by the duration of the direct irradiance as the CSP. Graphs in Figure 41 shows that even for very small direct irradiance, the PV system can still produce a decent amount of electricity.

Finally, in order to study the effect of the nameplate capacity, the AC annual system output, i.e. the total amount of electricity generated over the entire year, was used as reference. Its evolution is shown in Figure 42 and reveals that the electricity produced evolves proportionally with the Wdc installed of PV.

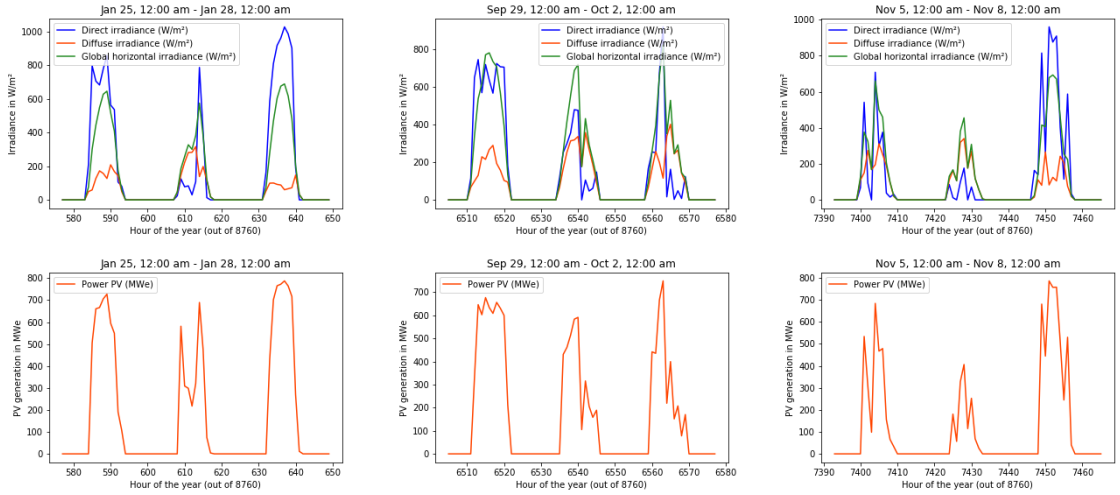

Figure 41: Evolution of the direct with the diffuse and the global horizontal irradiance (graphs above) and the power generated by the PV system (graphs below) at 3 different times of the year : from January 25^{th} to January 28^{th}, from September 29^{th} to October 2^{nd} and from November 5^{th} to November 8^{th}

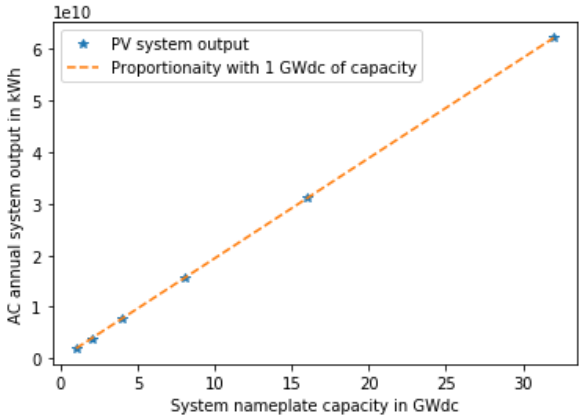

Figure 42: Evolution of the AC annual PV system output with respect to the system nameplate capacity

Part V
Models

11 Optimization PV - batteries - CSP

To solve the optimization problem in this study, mathematical programming is used. It is a field of applied mathematics that provides "a framework and solution methods for computing the decisions of an optimization problem, given an objective function to minimize or maximize, and constraints on the decisions variables" [32]. Gurobi is the solver used for the optimization. It allows to solve linear programming (LP), quadratic programming (QP), quadratically constrained programming (QCP), mixed integer linear programming (MILP), mixed-integer quadratic programming (MIQP), and mixed-integer quadratically constrained programming (MIQCP) [33].

This section presents the data, parameters, variables that will be optimized and constraints used in the optimization problem to size and simulate the electricity generation of each technology used. Each technology will be explained separately after presenting the objective function and key data and inputs for the entire model.

11.1 Index

Since SAM gives the PV production and the CSP generation on a hourly basis, the time step of the model of the optimization will also be the hour.

- t is the index of time period (corresponding in 1 hour), t = 1,..., $N_{Periods}$ where $N_{Periods} = 365 \cdot 24 = 8760$ is the number of periods the optimization is done on

11.2 Data and input of the model

As stated previously, the objective of the model is to meet the Belgium's demand in electricity using PV panels, batteries and CSP. The data for the Belgium's demand can be accessed from the Elia grid load data. Elia is the Belgium's transmission system operator and shares data of the evolution of the total Belgian electrical load in kW for any year since 2005. In order to optimize over an entire year, data from the year 2019 were selected [34]. However, the consumption is given every 15 minutes while the model works with an hourly time step. Therefore, the mean of the consumption of each hour was used as the load data.

For the CSP, the hourly thermal energy leaving in HTF and the hourly thermal energy charged from TES for a solar multiple of 1 and a nameplate capacity of 100 MW will be used as reference data. Then, the hourly generation of the CSP can be simulated for any size based on the expressions defined in the previous section. For the PV, the hourly electricity power generated from a 1 GWdc nameplate capacity is used as reference data.

The last key input of the model that needs to be determined is the technical lifetime of the model. Nowadays, CSP and PV panels have a technical lifetime of 25 years while the lifetime of a battery

varies between 10 and 15 years. Therefore, the technical lifetime chosen for the entire model is 25 years as the replacement of batteries will be taken into account in the model.

The notation for the data and input of the model are presented below :

- $Load_t$ in KWhe is the total load of the Belgium grid at time t
- $\dot{Q}_{HTF,out,SM=1,100MW,t}$ in MWht is the hourly maximum thermal energy leaving in HTF for $SM = 1$ and $W_{turb} = 100$ MWe at time t
- $\dot{Q}_{ch,SM=1,100MW,t}$ in MWht is the hourly maximum thermal energy charged in TES for $SM = 1$ and $W_{turb} = 100$ MWe at time t
- $PV_{1GW,t}$ in kWh is the hourly maximum production of energy from a PV system of 1 GWdc at time t
- $lifetime = 25$ is the technical lifetime of the entire model, i.e. the number of years the model will be used to produced electricity.

Therefore, $Load_t$, $\dot{Q}_{HTF,out,SM=1,100MW,t}$, $\dot{Q}_{ch,SM=1,100MW,t}$ and $PV_{1GW,t}$ are vectors of 8760 components. To account for the difference of time zones between Egypt and Belgium (UTC+2 for Egypt and UTC+1 for Belgium), the first components of the hourly reference data $\dot{Q}_{HTF,out,SM=1,100MW,t}$, $\dot{Q}_{ch,SM=1,100MW,t}$, $PV_{1GW,t}$ are given by the second hour of simulations from SAM. And the first hour of the simulation is relocated to the last component of each vector ($t = 8760$).

11.3 Objective function

The objective function chosen for this optimization problem is to minimize the price of the levelized total system cost, $LTSC$. The levelized total cost of the system allows to calculate the total cost of the system while taking into account the discount rate λ and the inflation rate d for project in a certain country. Equation (72) presents how the $LTSC$ is computed [10].

$$\min LTSC \tag{71}$$

where

$$LTSC = C_0 + OM_{cost} \cdot \frac{1}{\psi_\theta} \tag{72}$$

C_0 are the costs of installation of the system in \$. They are only paid the first year of the project. OM_{cost} are the cost related to the operation and maintenance (O&M) of the system in \$. They are paid during the entire lifetime of the system. Installation costs and O&M costs will both be calculated separately for each technology used in the system then add together as seen in Equations (73) and (74).

$$C_0 = C_{0,PV} + C_{0,storage} + C_{0,CSP} \tag{73}$$

$$OM_{cost} = OM_{PV} + OM_{storage} + OM_{CSP} \tag{74}$$

The discount rate is taken into account in the annuity factor, ψ. In order to consider the effect due to the inflation, the factor ψ_θ is used. Equations (75) to (77) [10] show how they are computed.

$$\psi = \frac{d}{1-(1+d)^{-lifetime}} \tag{75}$$

$$\psi_\theta = \frac{\theta}{1-(1+\theta)^{-lifetime}} \tag{76}$$

$$\theta = \frac{d-\lambda}{1+\lambda} \tag{77}$$

Despite installing the system in Egypt, since it produces electricity to meet the electricity demand of Belgium, the discount rate value chosen is the Belgian one [30] and the inflation rate was decided from the mean value of the inflation rate for the last 25 years in Belgium [29]. Table 20 presents the values of discount rate and inflation rate chosen and the annuity factor derived from those values.

	Notation	Value	Unit
Discount rate	d	0.75	%
Inflation rate	λ	2	%
Annuity	ψ	4.4	%
Annuity with inflation	ψ_θ	3.39	%

Table 20: Parameters used for the computation of the Levelized Total System Cost

11.4 CSP Model

11.4.1 Data used

- $\dot{Q}_{htf,out,SM=1,100MW,t}$ in MWht is the maximum thermal energy leaving in HTF for $SM = 1$ and $W_{turb} = 100$ MWe at time t
- $\dot{Q}_{ch,SM=1,100MW,t}$ in MWht is the maximum thermal energy charged in TES for $SM = 1$ and $W_{turb} = 100$ MWe at time t.

11.4.2 Parameters

The first parameters set relate to the sizing of the 3 main parts of the CSP : the solar field, the power cycle and the thermal storage. Moreover, since most of the equations defined in the previous part are bilinear, the nameplate capacity of each turbine is also fixed in the parameters.

- Parameters related to the solar field:
  - $DNI = 950$ W/m^2 is the direct normal irradiation at design
  - $\eta_{conv,loop} = 0.548$ is the total loop conversion efficiency
  - $A_{loop} = 5248$ m^2 is the single loop aperture
  - $L_{row} = 15$ m is the row spacing

- $W_{sca} = 6$ m is the aperture width
- $\eta_{non,sf} = 0.4$ is the non-solar field area multiplier

- Parameters related to the power cycle:
  - $CSP\_net\_output = [100; 300]$ Mwe is the nameplate capacity of each turbine used.
  - $\eta_{pc,gtn} = 0.9$ is the estimated gross to net conversion factor

- Parameters related to the thermal storage:
  - $\eta_{pc,th} = 0.356$ is the cycle thermal efficiency
  - $H_{tank} = 12$ m is the tank height
  - $N_{tank,pair} = 1$ is the number of tanks pair
  - $h_{tank,loss} = 0.4$ Wt/m^2-K is the tank thermal loss coefficient
  - $T_{TES,ave} = \frac{293+393}{2} + 273.15 = 616.15$ K is the average temperature of the thermal fluid in both tank
  - $Conv\_capacity\_volume = 20.91$ m^3/MWht is ratio between the volume of the tank and the thermal storage capacity using equation (20)
  - $CSP\_Initial\_SOC = 0.5$

In order to calculate $C_{0,CSP}$ and OM_{CSP}, several parameters need to be set related to the rated power of the CSP and multiple costs. The costs of installation are divided into 2 categories the direct capital costs and the indirect capital costs. The direct capital costs involve expense for a specific of piece of equipment or installation service. The indirect capital costs involve expense that cannot be associated with a specific piece of equipment or installation service. The parameters set are the following :

- Parameters related to the direct cost:
  - $CSP\_Storage\_cost = 62$ \$/kWht is the cost of the thermal storage
  - $CSP\_Field\_cost = 235$ \$/m^2 is the price related to any expense for the solar field
  - $CSP\_Power\_cost = 1000$ \$/kWe is the price related to the power block for each solar power plant for a power
  - $CSP\_Contingency = 7\%$ is a percentage of the 3 costs above to account for expected uncertainties in direct cost

- Parameters related to the indirect cost:
  - $CSP\_EPC\_cost = 11$ % of total direct cost is a percentage used to take into account engineer-procure-construct and owner costs. It includes costs such as permitting, consulting, management or legal fees, geotechnical and environmental surveys, interconnection costs, spare inventories, commissioning costs and the owner's engineering costs and project development activities
  - $CSP\_land\_cost = 10000$ \$/acre is the cost related to the land purchases
  - $CSP\_sales\_tax\_basis = 80$ % of total direct cost is the sales tax basis. Used with the sales tax rate, the total sales tax can be calculated.

- $CSP\_sales\_tax\_rate = 5$ % of total direct cost is the sales tax rate.

- Parameters related to the operation and maintenance
  - $CSP\_cost\_cap = 66$ \$/kW-yr is a fixed annual cost proportional to the system nameplate capacity
  - $CSP\_cost\_gen = 4$ \$/MWh is a variable annual cost proportional to the total annual electrical output

The values for those parameters are the one given by SAM by default. The operation and maintenance costs are assumed to cover every costs in order to avoid the deterioration of the electrical output trough the entire plant lifetime.

11.4.3 Variables

The parameters having been set, the variables on the model can be introduced. For the CSP, 12 variables are used. 5 sizing variables that will not depend on time t, 7 operation variables which values differ for each time t.

- Sizing variables :
  - $CSP\_TURB \in \mathbb{R}$ is the nameplate capacity of the entire installation in MWe made of turbines of size CSP_net_output
  - $CSP\_SM \in \mathbb{R}$ is the solar multiple of the entire installation based on the nameplate capacity of 1 turbine of size CSP_net_output
  - $CSP\_TES \in \mathbb{R}_{\geq 0}$ is the thermal storage capacity of the entire installation in MWht
  - $CSP\_A\_sf \in \mathbb{R}_{\geq 0}$ is the surface area of all mirrors of the solar field in m^2
  - $CSP\_A\_csp \in \mathbb{R}_{\geq 0}$ is the surface area of the entire installation in acre

- Operation variables:
  - $CSP\_SF\_out_t \in \mathbb{R}_{\geq 0}$ is the amount of thermal energy collected by the solar field at time t in MWht
  - $CSP\_W_{gen,t} \in \mathbb{R}_{\geq 0}$ is the amount of electricity generated at time t in MWhe
  - $CSP\_TES\_SOC_t \in \mathbb{R}_{\geq 0}$ is the state of charge of the thermal storage at time t in MWht
  - $CSP\_W_{cons,t} \in \mathbb{R}_{\geq 0}$ is the power consumed by the installation at time t in MWhe
  - $CSP\_TES\_disch_t \in \mathbb{R}_{\geq 0}$ is the thermal energy discharged from the thermal storage at time t in MWht
  - $CSP\_TES\_ch_t \in \mathbb{R}_{\geq 0}$ is the thermal energy charged into the thermal storage at time t in MWht
  - $CSP\_TES\_loss \in \mathbb{R}_{\geq 0}$ is the thermal energy lost from the thermal storage at each hour in MWht

11.4.4 Constraints

The constraints are the set of equations that variables are subjected to. In the CSP model, they defines how the CSP works with respect to its size.

Thermal energy leaving the solar field

As explained in the section about the data analysis and linearization, the hourly maximum thermal energy leaving from HTF is approximate using Equation (78). From that maximum value, lower values can be reached by defocusing mirrors, hence, decreasing the amount of sunlight used to heat the HTF. The reference data $\dot{Q}_{htf,out,SM=1,100MW,t}$ also helps to keep track on when the solar field receive direct irradiance ($\dot{Q}_{htf,out,SM=1,100MW,t} > 0$) and when it does not ($\dot{Q}_{htf,out,SM=1,100MW,t} \leq 0$ due to heat losses).

Moreover, an additional iterative variable SM_{iter} is used to take into account the effect of the solar multiple. The sizing variable CSP_SM determines the total solar multiple of the CSP for a turbine nameplate capacity of CSP_net_output. However, the total nameplate capacity of the CSP is given by the sizing variable CSP_TURB. Assuming that the solar multiple is equally divided between each turbine used to reach the total nameplate capacity, SM_{iter} is the number of solar multiple by turbine installed. Since the expressions linking thermal energy and power consumed to the solar multiple were determined for a turbine of capacity CSP_net_output, this is the solar multiple used by turbine that must be used.

For $t \in \mathrm{N}_{Periods}$,

if $\dot{Q}_{htf,out,SM=1,100MW,t} > 0$

$$CSP\_SF\_out_t \leq Ratio_{\dot{Q}_{htf},SM} \cdot \dot{Q}_{htf,out,W_{turb}} \tag{78}$$

where

$$Ratio_{\dot{Q}_{htf},SM} = \frac{CSP\_SM}{SM_{iter}} \cdot (0.862019 \cdot SM_{iter} + 0.301699) \tag{79}$$

$$\dot{Q}_{htf,out,W_{turb}} = \frac{0.919 \cdot CSP\_net\_output + 3.182}{0.919 \cdot 100 + 3.182} \cdot \dot{Q}_{htf,out,SM=1,100MW,t} \tag{80}$$

else,

$$CSP\_SF\_out_t = 0 \tag{81}$$

SM_{iter} is found by iteration by dividing total number of solar multiple used by the CSP by the number of turbines used once CSP_SM and CSP_TURB have been found by the optimization problem. The problem is optimized until the difference between SM_{iter} of 2 consecutive optimizations is smaller than 0.1.

Thermal energy charged in the thermal storage

The first constraint related to the thermal energy charged is that is should be smaller or equal to the thermal energy leaving in HTF. Then, to take into account parasitic effects discovered during the study in the previous section, equations from expressions (32), (33),(34) are also used.

For $t \in \mathrm{N}_{Periods}$,

$$CSP\_TES\_ch_t \leq CSP\_SF\_out_t \tag{82}$$

$$CSP\_TES\_ch_t \leq Ratio_{\dot{Q}_{ch},SM} \cdot \dot{Q}_{ch,W_{turb}} \tag{83}$$

where

$$Ratio_{\dot{Q}_{ch},SM} = \frac{CSP\_SM}{SM_{iter}} \cdot (0.869464 \cdot SM_{iter} + 0.288083) \tag{84}$$

$$\dot{Q}_{ch,W_{turb}} = \frac{0.902 \cdot CSP\_net\_output + 3.338}{0.902 \cdot 100 + 3.338} \cdot \dot{Q}_{ch,SM=1,100MW,t} \tag{85}$$

Thermal energy loss from the thermal storage

A type of losses that was not addressed yet is the thermal energy loss from the TES. In order to simulate this loss, an estimated value is used assuming that the tanks are 50 % charged. Similarly with the thermal energy leaving in HTF and the thermal energy charged, an iterative variable is used, TES_hours_{iter}. Assuming that an equal part of the total thermal storage capacity of the CSP is connected to each turbine, TES_hours_{iter} is the time of thermal storage at design point connected to each turbine.

From this variable and based on equations from SAM, the heat loss from tanks connected to one turbine $h_{tank,1}$ can be assessed using Equation (87). Then, by multiplying the heat loss from tanks connected to 1 turbine by the number of turbines, the total amount of thermal losses can be computed as seen in Equation (86). The number of turbines is found by dividing the total nameplate capacity of the CSP CSP_TURB by the nameplate capacity of one turbine CSP_net_output.

$$CSP\_TES\_loss = \frac{CSP\_TURB}{CSP\_net\_output} \cdot h_{tank,1} \tag{86}$$

where

$$h_{tank,1} = \left(H_{tank} \cdot \pi \cdot D_{tank,1} + \pi \cdot \left(\frac{D_{tank,1}}{2} \right) \right) \cdot N_{pair} \cdot (T_{TES,ave} - 20) \cdot \frac{h_{tank,loss}}{1e6} \tag{87}$$

$$D_{tank,1} = 2 \cdot \sqrt{\frac{V_{tes,1}}{H_{tank} \cdot \pi \cdot N_{pair}}} \tag{88}$$

$$V_{tes,1} = C_1 \cdot Conv\_capacity\_volume \tag{89}$$

$$C_1 = TES\_hours_{iter} \cdot \frac{CSP\_net\_output}{\eta_{pc,gtn} \cdot \eta_{pc,th}} \tag{90}$$

TES_hours_{iter} is found by iteration by dividing total thermal storage capacity used by the CSP by the number of turbines used once CSP_TES and CSP_TURB have been found by the optimization problem. The problem is optimized until the difference between TES_hours_{iter} of 2 consecutive optimizations is smaller than 0.1.

Thermal energy discharged from the thermal storage

For the thermal energy discharged from the TES, its only constraint is that it must be smaller that the state of charge of the TES.

For $t \in \mathrm{N}_{Periods}$,

$$CSP\_TES\_disch_t \leq CSP\_TES\_SOC_t \tag{91}$$

State of charge of thermal storage CSP

Now that the constraints about the thermal energy charged, discharged and lost from the TES have been established, the constraints about the state of charge of the TES can be defined. First, the state of charge must be smaller or equal to the thermal capacity of the CSP at all time. Then, the initial value of the thermal storage is capped by Equation (93). Finally, the evolution of the state of charge is given in Equation (94). Moreover, since the optimization is done for several years, the state of charge at the last hours of the year is the same than the first hour of the year to keep the continuity between consecutive years.

For $t \in \mathrm{N}_{Periods}$,

$$CSP\_TES\_SOC_t \leq CSP\_TES \tag{92}$$

if $t = 1$

$$CSP\_TES\_SOC_t \leq CSP\_Initial\_SOC \cdot CSP\_TES \tag{93}$$

else:

$$CSP\_TES\_SOC_t = CSP\_TES\_SOC_{t-1} - CSP\_TES\_disch_{t-1} + CSP\_TES\_ch_{t-1} - CSP\_TES\_loss \tag{94}$$

$$CSP\_TES\_SOC_{N_{Periods}} = CSP\_TES\_SOC_1 \tag{95}$$

Maximum thermal storage capacity

Since costs used come from the defaults values of SAM based on existing projects, the thermal storage capacity must be range in realistic values too. According to [35], thermal storage up to 15 hours TES capacity exist. Therefore, the thermal storage capacity was capped at 15 hours by turbine using equation (96)

$$\frac{CSP\_TES}{TES\_max} \leq \frac{CSP\_TURB}{CSP\_net\_output} \tag{96}$$

where

$$TES\_max = 15 \cdot \frac{CSP\_net\_output}{\eta_{pc,gtn} \cdot \eta_{pc,th}} \tag{97}$$

Generation CSP

For the generation of CSP, the first constraint limits the maximum power to grid than can be sent for any hour by the total nameplate capacity of the turbine. Other constraints relate to the power generated from the thermal energy coming from the solar field and the thermal energy storage using the equations defined in the subsections 9.5.3 and 9.5.4.

For $t \in \mathrm{N}_{Periods}$,

$$CSP\_W_{gen,t} \leq CSP\_TURB \tag{98}$$

Assuming that any value of electric power produced by the CSP can be reached by a combination of turbines running either above 20% of their nameplate capacity or not used,

$$CSP\_W_{gen,t} = \dot{W}_{TES} + \dot{W}_{SF} \tag{99}$$

where $\dot{W}_{TES}$ is the amount of electricity converted from the thermal energy coming from the TES and computed using Equation (100) and $\dot{W}_{SF}$ is the amount of electric power converted from the thermal energy directly leaving from HTF and computed using Equation (101).

$$\dot{W}_{TES} = 0.398 \cdot CSP\_TES\_disch_t + (-0.414 - 0.082 \cdot CSP\_net\_output) \tag{100}$$

$$\dot{W}_{SF} = (-0.000026 \cdot CSP\_net\_output + 0.395) \cdot \dot{Q}_{htf,out,W_{grid}} + (-0.089 \cdot CSP\_net\_output - 0.916) \tag{101}$$

$$\dot{Q}_{htf,out,W_{grid}} = \dot{Q}_{htf,out,W_{turb},SM} - \dot{Q}_{ch,W_{turb},SM} \tag{102}$$

Power consumed by the plant

Constraints related to the power consumed use also equations define in the Data analysis and linearization part. Moreover, to take into account the impact on solar multiple, the slope and the intercept of Equations (104) and (107) vary depending on the value of SM_{iter}.

For $t \in \mathrm{N}_{Periods}$,

if $Hours_t \geq 6$ and $Hours_t < 20$:

$$CSP\_W_{cons,t} = Ratio_{\dot{W}_{cons,day},SM} \cdot \dot{W}_{cons,day,W_{turb}} \tag{103}$$

where

$$Ratio_{\dot{W}_{cons,day},SM} = \frac{CSP\_SM}{SM_{iter}} \cdot (slope_{day} \cdot SM_{iter} - intercept_{day}) \tag{104}$$

$$\dot{W}_{cons,day,W_{turb}} = (-0.569 + 0.013 \cdot CSP\_net\_output) \tag{105}$$

if $Hours_t \geq 20$ or $Hours_t < 6$:

$$CSP\_W_{cons,t} = Ratio_{\dot{W}_{cons,night},SM} \cdot \dot{W}_{cons,night,W_{turb}} \tag{106}$$

$$Ratio_{\dot{W}_{cons,night},SM} = \frac{CSP\_SM}{SM_{iter}} \cdot (slope_{night} \cdot SM_{iter} - intercept_{night}) \tag{107}$$

$$\dot{W}_{cons,night,W_{turb}} = (0.000034 \cdot CSP\_net\_output - 0.0017) \tag{108}$$

where $Hours_t$ is the hour of the day at time t. Its values vary from 0 to 23 in increments of 1.

SM_{iter}	$slope_{day}$	$intercept_{day}$	$slope_{night}$	$intercept_{night}$
$\mathbf{1} \leq SM_{iter} \leq \mathbf{2}$	1	0	1.23249	- 0.229621
$\mathbf{2} < SM_{iter} \leq \mathbf{3}$	1	0	1.232490	- 0.229621
$\mathbf{3} < SM_{iter} \leq \mathbf{4}$	1	0	1.232490	- 0.229621
$\mathbf{4} < SM_{iter} \leq \mathbf{5}$	1	0	1.640239	- 1.851743
$\mathbf{5} < SM_{iter} \leq \mathbf{6}$	1	0	1.640239	- 1.851743
$\mathbf{6} < SM_{iter} \leq \mathbf{7}$	1	0	1.640239	- 1.851743
$\mathbf{7} < SM_{iter} \leq \mathbf{8}$	1	0	1.640239	- 1.851743
$\mathbf{8} < SM_{iter} \leq \mathbf{9}$	3.776515	- 21.802248	2.860630	- 11.486026
$\mathbf{9} < SM_{iter} \leq \mathbf{10}$	3.776515	- 21.802248	2.860630	- 11.486026
$\mathbf{10} < SM_{iter} \leq \mathbf{11}$	1.942354	- 3.849975	2.860630	- 11.486026
$\mathbf{11} < SM_{iter} \leq \mathbf{12}$	1.942354	- 3.849975	2.860630	- 11.486026
$\mathbf{12} < SM_{iter} \leq \mathbf{13}$	1.942354	- 3.849975	2.860630	- 11.486026
$\mathbf{13} < SM_{iter}$	1.942354	- 3.849975	2.860630	- 11.486026

Table 21: Values of the slopes and the intercepts for the equations assessing the power consumed during night and day for each value of solar multiple

Solar field area

The solar field area is the total reflective aperture area is assessed based on equations used in SAM. It expresses the amount of collectors used in m^2.

$$CSP\_A\_sf = A_{tot,SCA} \tag{109}$$

where

$$A_{tot,SCA} = N_{loop} \cdot A_{loop} \tag{110}$$

$$N_{loop} = round\left(CSP\_SM \cdot \frac{A_{tot,SCA,SM=1}}{A_{loop}}\right) \tag{111}$$

$$A_{tot,SCA,SM=1} = \frac{\dot{Q}_{th,pc}}{\eta_{conv,loop} \cdot DNI} \cdot 1e6 \tag{112}$$

$$\dot{Q}_{th,pc} = \frac{CSP\_net\_output}{\eta_{pc,th} \cdot \eta_{pc,gtn}} \tag{113}$$

CSP area

The CSP area is the total area covered by the CSP and it is assessed based on equation used in SAM.

$$CSP\_A\_csp = CSP\_A\_sf \cdot \frac{L_{row}}{W_{sca}} \cdot (1 + \eta_{non,sf}) \cdot 0,000247105 \tag{114}$$

11.4.5 Costs

As stated in the explanation of the parameters of the CSP model, the costs of installation for the CSP are divided into 2 categories : the direct capital costs and the indirect capital costs. As for the operation and maintenance costs, they are assessed using Equation (119). The first term is a fixed operation maintenance cost (FOM) proportional to the installed capacity of the CSP while the second term is variable operation maintenance cost (VOM) proportional to the total power generated from the CSP.

$$C_{0,CSP} = Direct\_cost + Indirect\_cost \tag{115}$$

$$Direct\_cost = Subtotal + CSP\_contingency \cdot Subtotal \tag{116}$$

$$\begin{aligned} Subtotal = & \, CSP\_A\_sf \cdot CSP\_Field\_cost \\ & + CSP\_TES \cdot CSP\_Storage\_cost \cdot 1000 \\ & + \frac{CSP\_TURB}{\eta_{pc,gtn}} \cdot CSP\_Power\_cost \cdot 1000 \end{aligned} \tag{117}$$

$$\begin{aligned} Indirect\_cost = & \, CSP\_A\_csp \cdot CSP\_land\_cost \\ & + Direct\_cost \cdot CSP\_EPC\_cost \\ & + Direct\_cost \cdot CSP\_sales\_tax\_basis \cdot CSP\_sales\_tax\_rate \end{aligned} \tag{118}$$

$$\begin{aligned} OM_{CSP} = & \, CSP\_TURB \cdot CSP\_cost\_cap \cdot 1000 \cdot lifetime \\ & + CSP\_cost\_gen \cdot \sum_{t=1}^{N_{Periods}} CSP\_generation_t \cdot lifetime \end{aligned} \tag{119}$$

11.5 PV Model

11.5.1 Data used

- $PV_{1GW,t}$ in kWh is the maximum production of energy from PV for 1 GWdc at time t

11.5.2 Parameters

Parameters used for the PV system relate to its costs and its performance deterioration. The installed cost account for the module and the inverter price and used SAM default values. Moreover, to take into account the use of tracker, the installed cost was multiplied by 1.2 and the maintenance cost by 1.1.

- $Installed\_cost = 0.96 \cdot 1.2$ \$/Wdc of PV
- $Maintenance_{cost,PV} = 13 \cdot 1.1$ \$/kW-yr
- $Deterioration_{PV} = 0.5$ %/year

11.5.3 Variables

4 variables are used for the PV model, 1 sizing variable and 3 operation variables.

- Sizing variable :
  - $PV_{capacity}$ in MWdc $\in \mathbb{R}_{\geq 0}$ is the PV system capacity installed
- Operation
  - $PV_{generation,t} \in \mathbb{R}_{\geq 0}$ in MWhe is the amount of energy used at time t
  - $PV_{production,t} \in \mathbb{R}_{\geq 0}$ in MWhe is the maximum energy that could produced by the PV panels at time t
  - $PV_{curtailment,t} \in \mathbb{R}_{\geq 0}$ in MWhe is the amount of energy curtailed from the $PV_{production,t}$ at time t

11.5.4 Constraints

PV production rule 1

The first constraint determines the maximum production of energy that could be generated by the PV system depending on the PV system nameplate capacity.

For $t \in \mathrm{N}_{Periods}$,

$$PV_{production,t} = PV_{capacity} \cdot \frac{PV_{1GW,t}}{1e6} \tag{120}$$

PV production rule 2

The second constraint defines the relation between the maximum production of energy that could be generated from the PV system, the amount of energy used from the PV system and the amount of energy curtailed from the PV system.

For $t \in \mathrm{N}_{Periods}$,

$$PV_{production,t} = PV_{generation,t} + PV_{curtailment,t} \tag{121}$$

11.5.5 Costs

Finally, the costs are assessed using Equations (122) and (123). For the OM costs, the second term of the equation accounts for the capacity added every year in order to be able to produced the same amount of electricity despite the deterioration of performance.

$$C_{0,PV} = PV_{capacity} \cdot Installed\_cost \cdot 1e6 \tag{122}$$

$$\begin{aligned} OM_{PV} = {} & OM\_cost\_PV \cdot 1000 \cdot PV_{capacity} \cdot lifetime \\ & + Deterioration_{PV} \cdot PV_{capacity} \cdot Installed\_cost \cdot 1e6 \cdot (lifetime - 1) \end{aligned} \tag{123}$$

11.6 Batteries

11.6.1 Parameters

Since battery storage costs have evolved rapidly over the recent years, parameters for the battery are based on a paper about the cost projections for utility-scale battery storage from the NREL [31]. In this paper, cost projections for a 4-hour duration lithium-ion battery systems from 2020 to 2050 are documented from several publications. A low, mid and high cost projection are then developed from the published values. Using the mid cost projections developed in this work in $/kWh, and assuming a 15 years storage lifetime, the costs of installation were chosen for the years 2020 and 2035. Indeed, since the storage lifetime is 15 years, batteries will need to be replaced once during the technical lifetime of the installation (25 years). Therefore, the costs of battery will have decrease by the time they replaced. The costs take into account the price of the battery with the price of power components such as the inverters.

As for the O&M costs, based on the same paper from the NREL, a value of 2.5 % of the $/kW capacity cost was selected. The capacity cost in $/kW is determined by multiplying the costs in $/kWh by the number of hours of storage. Moreover, it is assumed that the O&M costs will counteract the degradation of the battery storage by including some capacity additions or replacements.

Additional parameters related to the round-trip efficiency and the initial value of the storage need also to be set. A round-trip efficiency of 85 % was chosen, represented by a charge and discharge efficiency of 92.2 % (since the root square of 0.85 is 0.922).

- $Battery\_storage\_cost$ = 330 and 194 $/kWh are the costs of installation of the battery storage for 4-hour lithium-ion system in 2020 and 2035 respectively
- $Battery\_storage\_OM\_cost$ = 33 and 19.4 $/kW are the O&M costs of the battery storage for a 4-hour lithium-ion system in 2020 and 2035 respectively
- $Initial_{soc}$ = 50 % is the initial value of the storage
- $charge\_efficiency = 0.922$
- $discharge\_efficiency = 0.922$
- $Storage\_lifetime$ = 15 years

11.6.2 Variables

5 variables are optimized for the battery, 2 sizing variables and 3 operation variables.

- Sizing variables :
  - $storage\_capacity \in \mathbb{R}_{\geq 0}$ is the maximum capacity of the batteries in MWh
  - $storage\_power \in \mathbb{R}_{\geq 0}$ is the maximum rated power of the batteries in MW
- Operation variables :
  - $SOC\_storage_t \in \mathbb{R}_{\geq 0}$ is the state of charge at time t in MWh
  - $charge\_storage_t \in \mathbb{R}_{\geq 0}$ is the amount of energy charged at time t in MWh
  - $discharge\_storage_t \in \mathbb{R}_{\geq 0}$ is the amount of energy charged at time t in MWh

11.6.3 Constraints

State of charge of the battery system

Similarly with the thermal storage of the CSP, the state of charge of the battery must be smaller or equal to the maximum capacity of the battery. The initial value of the battery is capped by Equation (125). Taking into account the charge and the discharge of the battery, the evolution of the state of charge is given in Equation (126). Finally, to keep the continuity of the state of charge between consecutive years, the state of charge at the end of a year is fixed at the same value than the state of

charge in the beginning of the year.

For $t \in \mathrm{N}_{Periods}$,

$$SOC\_storage_t \leq storage\_capacity \tag{124}$$

if $t = 1$:

$$SOC\_storage_t \leq Initial\_soc \cdot storage\_capacity \tag{125}$$

else :

$$\begin{aligned} SOC\_storage_t = {} & SOC\_storage_{t-1} \\ & + charge\_efficiency \cdot charge\_storage_t \\ & - \frac{1}{discharge\_efficiency} \cdot discharge\_storage_t \end{aligned} \tag{126}$$

$$SOC\_storage_{N_{Periods}} = Initial\_soc \cdot storage\_capacity \tag{127}$$

Storage power rule

Since costs are based on 4-hour duration systems, the storage rated power must equal to 1 quarter of the storage capacity.

$$storage\_power = \frac{storage\_capacity}{4} \tag{128}$$

Charge/discharge rule

The charge and discharge are capped by the maximum rated storage power.
For $t \in \mathrm{N}_{Periods}$,

$$charge\_storage_t + discharge\_storage_t \leq storage\_power \tag{129}$$

Charge PV rule

The charge is also capped by the production of PV.

For $t \in \mathrm{N}_{Periods}$,

$$charge\_storage_t \leq PV_{generation,t} \tag{130}$$

Discharge rule

The discharge by the amount of energy left in the battery.

For $t \in \mathrm{N}_{Periods}$,

$$discharge\_storage_t \leq SOC\_storage_t \tag{131}$$

11.6.4 Costs

Finally, the costs of installation and the costs of operation and maintenance are given in Equations (132) and (133). The index added to the parameters related to the costs refers to year of installation of the battery storage. The second term and third term of the O&M costs account for the maintenance cost of the battery storage replaced and the price of the replacement taking into account the evolution of costs of the battery storage.

$$C_{0,storage} = Battery\_storage\_cost_{2020} \cdot 1000 \cdot storage\_capacity \tag{132}$$

$$\begin{aligned} OM_{storage} = {} & Battery\_storage\_OM\_cost_{2020} \cdot 1000 \cdot storage\_power \cdot Storage\_lifetime \\ & + Battery\_storage\_OM\_cost_{2035} \cdot 1000 \cdot storage\_power \cdot (lifetime - Storage\_lifetime) \\ & + Battery\_storage\_cost_{2035} \cdot 1000 \cdot storage\_capacity \end{aligned} \tag{133}$$

11.7 Power balance rule

The power balance rule is the main constraint the model must respect at every moment. It is presented in Equation (134). It assures that the Belgian consumption is met by the electricity production from the PV, the CSP and the batteries.

For $t \in \mathrm{N}_{Periods}$,

$$PV_{generation,t} + discharge\_storage_t + CSP\_W_{gen,t} = Load_t \cdot 1000 + charge\_storage_t + CSP\_W_{cons,t} \tag{134}$$

Part VI
Results and analysis

12 Results

This section presents the results of the optimization problem. To clearly evaluate the effects of combining the PV system, the battery storage and the CSP, the first optimizations are done using either the PV and battery only or the CSP to meet the Belgian demand. To compare the results, for each simulation, the levelized cost of electricity $LCOE$ is evaluated. The levelized cost of electricity in \$/MWh can be calculated using equation (135) [10] where the investment horizon refers to how long investors expect their money to remain invested before they cash it in.

$$LCOE = \frac{LTSC \cdot \psi}{\sum_{t=1}^{N_{Periods}} \frac{Load_t}{1000} \cdot Investment\_horizon} \tag{135}$$

Moreover, to gain a better understanding of the source of the costs, the capital expenditures, $CAPEX$ and the operational expenditures, $OPEX$, are also computed for each optimization. The capital expenditures are related to the installation costs C_0 and are given in \$/MWh using Equation (136) [10].

$$CAPEX = \frac{C_0 \cdot \psi}{\sum_{t=1}^{N_{Periods}} \cdot Investment\_horizon} \tag{136}$$

The operational expenditures are related to the operation and maintenance costs OM_{cost} and can be computed in \$/MWh using equation (137) [10].

$$OPEX = \frac{OM \cdot \frac{\psi}{\psi_\theta}}{\sum_{t=1}^{N_{Periods}} \frac{Load_t}{1000} \cdot Investment\_horizon} \tag{137}$$

12.1 PV-battery system only

Table 22 presents the results of the optimization using only the PVs and the battery systems to meet the Belgian electricity demand. An investment horizon of 25 years was chosen to compute the LCOE. Moreover, the capex, the opex and LCOE were also computed separately for the PV and the battery to analyze how each of them affect the LCOE. Equations (138) to (143) show how they are computed, dividing their respective costs by the respective amount of electricity they have generated. From the costs given in the Table 22, it can be concluded that it is the battery storage that is the main cause of the LCOE for the PV-battery system.

$$CAPEX\_PV = \frac{C_{0,PV} \cdot \psi}{\sum_{t=1}^{N_{Periods}} PV_{generation,t} \cdot Investment\_horizon} \tag{138}$$

$$OPEX\_PV = \frac{OM_{PV} \cdot \frac{\psi}{\psi_\theta}}{\sum_{t=1}^{N_{Periods}} PV_{generation,t} \cdot Investment\_horizon} \tag{139}$$

$$LCOE\_PV = CAPEX\_PV + OPEX\_PV \tag{140}$$

$$CAPEX\_storage = \frac{C_{0,storage} \cdot \psi}{\sum_{t=1}^{N_{Periods}} discharge\_storage_t \cdot Investment\_horizon} \tag{141}$$

$$OPEX\_storage = \frac{OM_{storage} \cdot \frac{\psi}{\psi_\theta}}{\sum_{t=1}^{N_{Periods}} discharge\_storage_t \cdot Investment\_horizon} \tag{142}$$

$$LCOE\_storage = CAPEX\_storage + OPEX\_storage \tag{143}$$

PV capacity [GWdc]	150.55
Storage capacity [GWh]	212.03
Storage Power [GW]	53.01
CAPEX PV storage [$/MWh]	2.35
OPEX PV storage [$/MWh]	104.53
LCOE PV storage [$/MWh]	**110.20**
capex PV [$/MWh]	3.65
opex PV [$/MWh]	46.32
LCOE PV [$/MWh]	**49.98**
capex storage [$/MWh]	2.71
opex storage [$/MWh]	88.57
LCOE storage [$/MWh]	**91.28**

Table 22: Results of the optimization using PVs and battery storage systems only to meet the Belgium demand

Furthermore, since the capacity of the PV is 150.55 GWdc while the peak in demand in electricity in Belgium is around 13 GWe, electricity produced by the PVs are mainly used to charge the battery. This observation is confirmed by looking at the evolution of the hourly state of charge, electricity charged and discharged in the battery storage in the graphs of Figure 43. When the battery is charging, the energy charged roughly averages 50 GWe, far higher than the Belgian consumption. However, when the battery is discharging, it only averages 10 GWe and follows the Belgian consumption, usually during nighttime.

As for the generation of electricity by the PVs, graphs on Figure 44 show that a large part is curtailed. Looking at the graph on the right of Figure 44, it can be seen that at the beginning of each day, PVs are only used to meet the Belgian demand. It is only during a handful of hours than PV generate at a higher capacity in order to charge the battery.

Usually, the energy charged during day is completely discharged during night as seen in the graph on the right of Figure 43. However, there are days for which the energy produced by the PV on one day is not enough to charge the battery and meet the Belgian demand during night. The battery is therefore charged at higher values on the previous days to be sure to have enough energy for every night as seen in Figure 45.

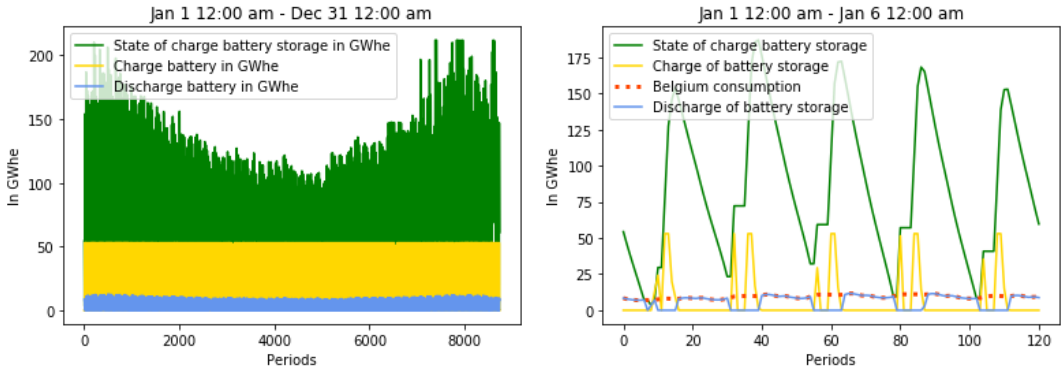

Figure 43: Evolution of the state of charge of the battery, the energy charged and the energy discharged over the entire year on the graph on the left and from January 1^{st} to 6^{th} with the Belgian consumption of the graph on the right from the optimization results when the PV-battery system is used alone

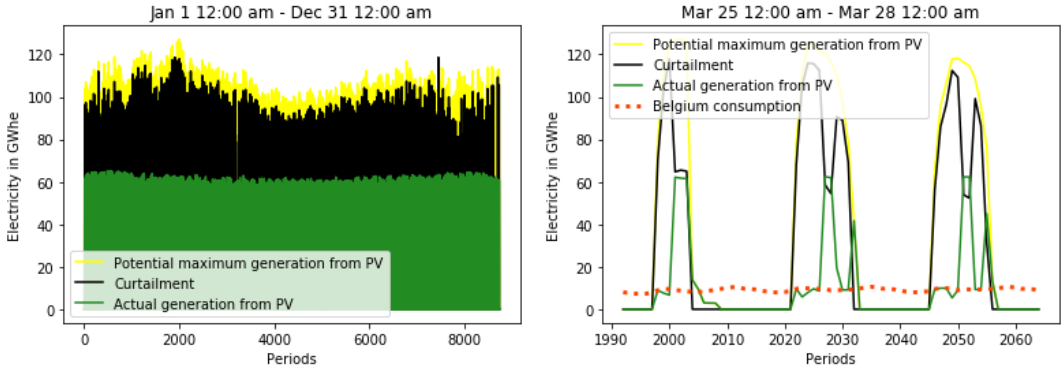

Figure 44: Evolution of the electricity generated and curtailed over the entire year (on the left graph) and from March 25^{th} to 28^{th} (on the right graph) from the optimization results when the PV-battery system is used alone

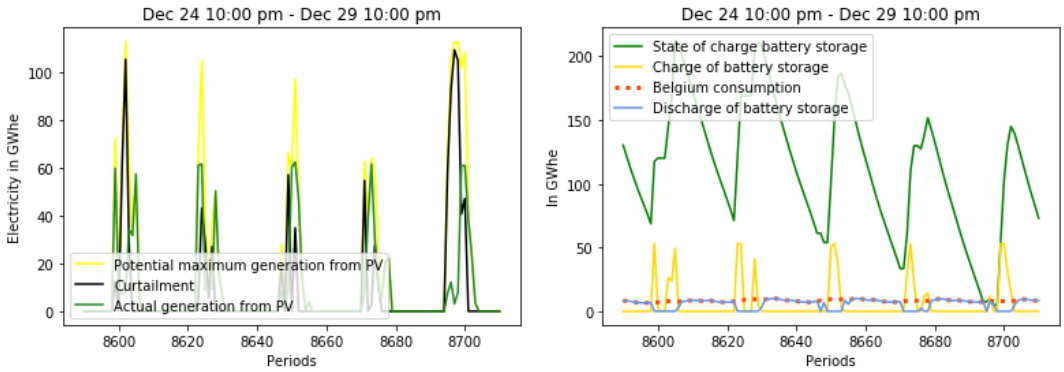

Figure 45: Evolution of the electricity generated and curtailed from December 24^{th} to 29^{th} (on the left graph) and evolution of the state of charge of the battery, the energy charged and the energy discharged from December 24^{th} 1^{st} to 29^{th} with the Belgian consumption from the optimization results when the PV-battery system is used alone

12.2 CSP only

For the CSP, the optimizations were done for different nameplate capacity by turbine. From Table 23 presenting the results of the different optimizations, it can be noticed that the higher the nameplate capacity used by turbine, the more expensive the cost of electricity of the CSP is. The capex for CSP are higher than for the PV-battery systems but the opex are far lower, as the CSP does not need yearly replacement for a part of its capacity.

Nameplate capacity by turbine [GWe]	**100**	**200**	**300**
Total nameplate capacity [GWe]	52.4	54	54.6
Solar field area [km²]	931.90	973.33	988.68
Solar multiple by turbine	2.97	3.01	3.03
Thermal energy storage capacity [GWht]	2454.28	2521.40	2,546.82
Hours of storage by turbine	15	15	15
CSP area [km²]	3261.64	3406.66	3460.39
capex CSP [$/MWh]	12.51	12.96	13.13
opex CSP [$/MWh]	65	66.81	67.49
LCOE CSP [$/MWh]	77.51	79.77	80.62

Table 23: Results of the optimization using only the CSP to meet the Belgium demand

The differences in cost are mainly due to the increase in the power consumed by the CSP as the nameplate capacity by turbine increases. Indeed, from the same graph generated in section 9.3.5, it can be seen that the evolution of the mean of power consumed during day is steeper than if the evolution was proportional with the mean of power consumed for a nameplate capacity of 100 MW in Figure 46. To compensate this increase in power consumed, the total nameplate capacity of the CSP is slightly increased as the nameplate capacity by turbine increases.

The 2 graphs on Figure 47 display the evolution of the state of charge of the TES of the CSP, the thermal energy charged and the thermal energy discharged for a nameplate capacity by turbine of 100 MW. As can be seen, the TES reachs its highest values during the last quarter of the year. Similarly with the battery storage in the PV-battery system, the TES is highly charged at this period to compensate the lack of direct irradiation and therefore, thermal energy collected by the solar field. It is illustrated in the graph on the right of Figure 47 where low to no thermal energy in charged in the TES on several occasions.

For the evolution of thermal energy collected by the solar field, the graphs on Figure 48 display the evolution of the thermal energy leaving in HTF, which is either stored in the TES or directly used to generate electricity. This evolution is compared with the maximum thermal energy that could have been collected if the collectors were used at their full potential.

As can be seen on the left graph of Figure 48, the solar field collects as much as thermal energy as it can in the beginning and the end of the year. For the rest of the year, especially between the 2000^{th}

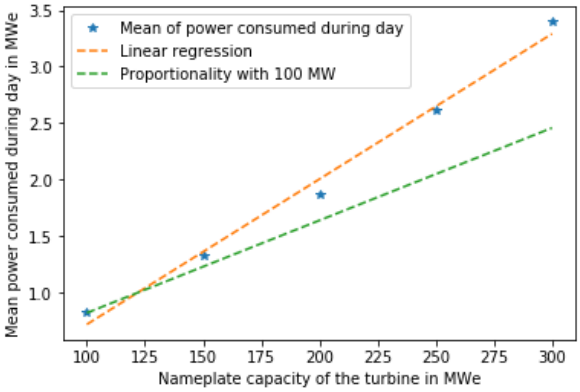

Figure 46: Evolution of the mean of the power consumed during day with respect to the nameplate capacity of the turbine

and the 6000^{th} hours of the year, only a small fraction of the potential maximum thermal energy is collected by the solar field. Therefore, for a large part of the year, the CSP is oversized.

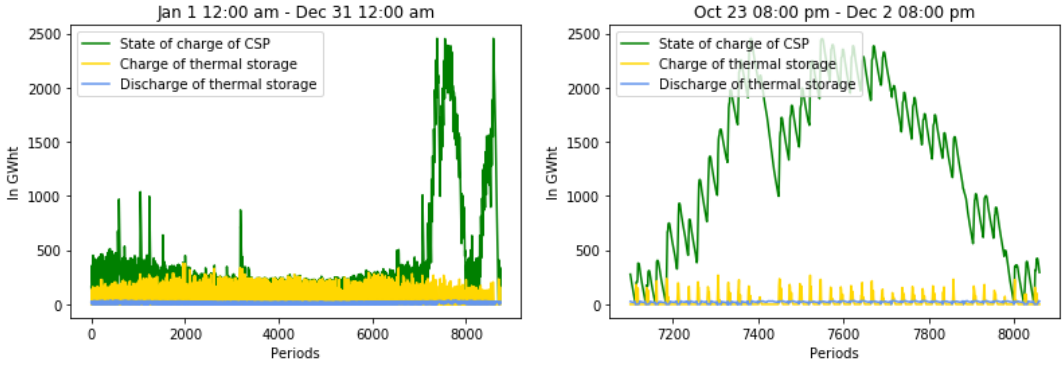

Figure 47: Evolution of the state of charge of the CSP, the energy charged and the energy discharged over the entire year on the graph on the left and from October 23^{th} to December 2^{nd} on the graph on the right from the optimization results when the CSP is used alone to meet the Belgium demand

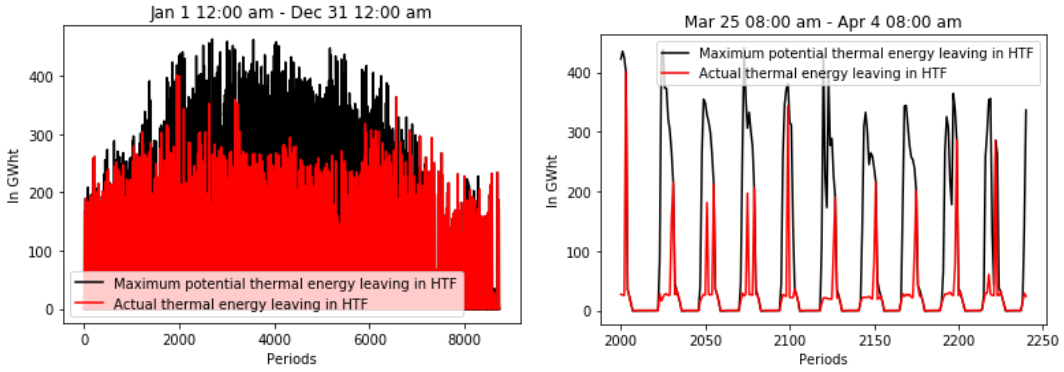

Figure 48: Evolution of the potential maximum thermal energy leaving in HTF and the actual thermal energy leaving in HTF over the entire year on the graph on the left and from March 25^{th} to April 4^{th} on the graph on the right from the optimization results when the CSP is used alone to meet the Belgium demand

12.3 PV-battery and CSP together

For the optimizations using PVs, battery storage and CSP, a nameplate capacity by turbine of 100 MW was used for the CSP. Moreover, the capex, the opex and LCOE were also computed separately for the CSP and the PV- battery to analyze how efficiently they will be used for their respective capacity installed. Equations (144) to (149) shows how they are computed, dividing their respective costs by the respective amount of electricity they generated.

$$CAPEX\_PV\_storage = \frac{(C_{0,PV} + C_{0,storage}) \cdot \psi}{\sum_{t=1}^{N_{Periods}} (PV_{generation,t} + discharge\_storage_t - charge\_storage_t) \cdot Investment\_horizon} \tag{144}$$

$$OPEX\_PV\_storage = \frac{(OM_{PV} + OM_{storage}) \cdot \frac{\psi}{\psi_\theta}}{\sum_{t=1}^{N_{Periods}} (PV_{generation,t} + discharge\_storage_t - charge\_storage_t) \cdot Investment\_horizon} \tag{145}$$

$$LCOE\_PV\_storage = CAPEX\_PV\_storage + OPEX\_PV\_storage \tag{146}$$

$$CAPEX\_CSP = \frac{C_{0,CSP} \cdot \psi}{\sum_{t=1}^{N_{Periods}} (CSP\_W_{gen,t} - CSP\_W_{cons,t}) \cdot Investment\_horizon} \tag{147}$$

$$OPEX\_CSP = \frac{OM_{CSP} \cdot \frac{\psi}{\psi_\theta}}{\sum_{t=1}^{N_{Periods}} (CSP\_W_{gen,t} - CSP\_W_{cons,t}) \cdot Investment\_horizon} \tag{148}$$

$$LCOE\_CSP = CAPEX\_CSP + OPEX\_CSP \tag{149}$$

Table 24 presents the results of the optimization problems when the PV, the battery and the CSP are used. 2 scenario were generated. The first scenario does not impose any limit on the nameplate capacity of the CSP. It allows the optimization to oversize it in order to increase the total TES capacity of the CSP. As can be seen in the Table, in this scenario, the TES of the CSP is used as the only storage medium. However, the total nameplate capacity reachs 43.7 GW which is far higher than the average Belgian electricity consumption. From this results, it can be deduced than a large part of the turbines installed will remain unused or used at a charge load far lower than their design point for the major part of the year. Moreover, the surface area needed to collect the necessary thermal energy is gigantic (2394.98 km^2 is almost 8 % of the total surface of Belgium, bigger than the Brabant wallon), making its maintenance very difficult. Finally, the amount of thermal energy storage.

The second scenario proposes a more down-to-earth result by limiting the nameplate capacity of the CSP at 15 GW, a value close to the maximal Belgian consumption. This limitation causes a limitation in the thermal storage capacity. To compensate, battery storage are also used. It increases the costs of electricity but allows a more realistic combination of technologies. This section will present a thorough

CSP		
Limit on the nameplate capacity	**No limit**	**15 GW**
Total nameplate capacity [GWe]	43.70	15
Solar field area [km²]	684.25	237.12
Solar multiple by turbine	2.61	2.64
Thermal energy storage capacity [GWht]	2454.28	702.25
Hours of storage by turbine	15	15
CSP area [km²]	2394.89	829.91
capex CSP [$/MWh]	16.37	31.95
opex CSP [$/MWh]	88.58	167.15
LCOE CSP [$/MWh]	104.95	199.10
PV-battery system		
PV capacity [GWdc]	20.79	79.07
Storage capacity [GWh]	0.00	106.87
Storage power [GW]	0.00	26.72
capex PV storage [$/MWh]	1.39	1.46
opex PV storage [$/MWh]	17.59	60.12
LCOE PV storage [$/MWh]	18.98	63.41
Final costs		
CAPEX $/MWh	10.34	6.32
OPEX $/MWh	60.00	71.42
LCOE $/MWh	**70.35**	**77.74**

Table 24: Results of the optimization problem using the PV, the battery and the CSP

analysis of the results for the second scenario.

As a first observation, the LCOE of the PV-battery have decreased comparing to the case when they were used alone (from 110.2 $/MWh to 63.41 $/MWh). This drop in the costs related to the PV-battery system is due to the high usage of the battery storage and the decrease in electricity curtailed from the PV as seen in Figure 49. Indeed, unlike when used only with the PV, the battery is charged at its full capacity almost everyday. The PVs are still curtailed but at a smaller fraction than when used with the battery only.

As for the LCOE related the CSP, it has increased compared to the LCOE when the CSP was used alone to meet the Belgian demand. Graphs of Figure 50 show that the CSP is mainly used during the beginning and the end of the year. Indeed, the actual thermal energy leaving in HTF is very closed to maximum potential thermal leaving in HTF at those time of the year. However, for the rest of the year, the fraction of actual thermal energy collected by the solar field is lower than when the CSP was used alone. Moreover, the thermal energy charged in the TES reaches higher values at the beginning and the end of the year. Similarly to when the CSP was used alone to meet the Belgian demand, the peak values of the thermal storage are reached in the last quarter of the year as the optimization anticipate the lack of direct irradiance on certain days for this period of the year.

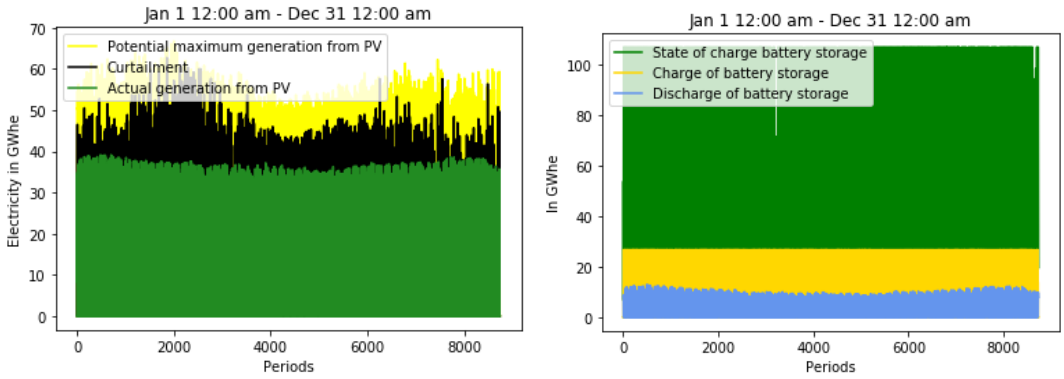

Figure 49: Evolution of the electricity generated and curtailed over the entire year (on the left graph) and evolution of the state of charge of the battery, the energy charged and the energy discharged over the entire year (on the graph on the right) and evolution of the state of charge of the CSP, the energy charged and the energy discharged over the entire year on the right from the optimization results using all production means

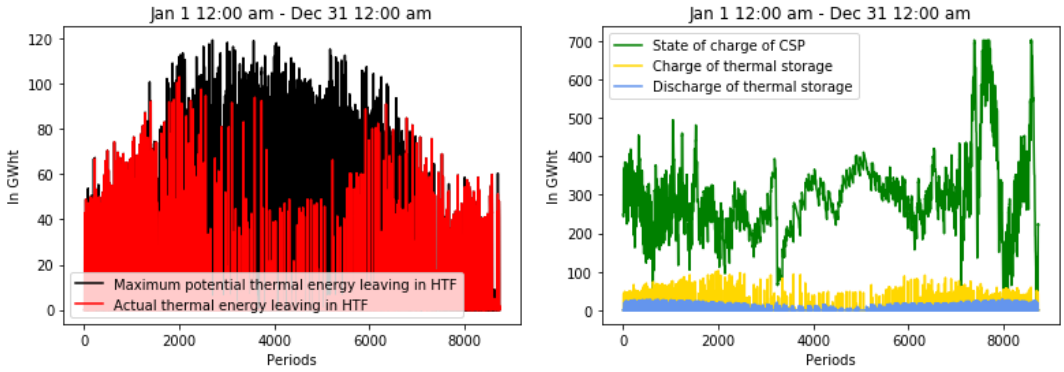

Figure 50: Evolution of the maximum potential thermal energy leaving in HTF and the actual thermal energy leaving in HTF over the entire year on the left graph and evolution of the state of charge of the CSP, the thermal energy charged and the thermal energy discharged over the entire year on the graph on the right from the optimization results using all production means

Moreover, from the graph of Figure 51. it can be seen that the CSP is only used as a thermal storage. Indeed, no electricity is generated from the conversion of thermal energy coming from the solar field. CSP seems to assist the PV-battery system when the Belgian consumption is at its highest values (therefore in Winter). It is illustrated on graphs of Figures 52 and 53. During a period of high demand, such as in January, the production of electricity during night is distributed between the CSP and the battery as the battery does not have enough capacity to take care of it by itself. However, during a period of lower demand, such as in July, the capacity of the battery storage is enough to deliver enough electricity by itself before being charged for the next day.

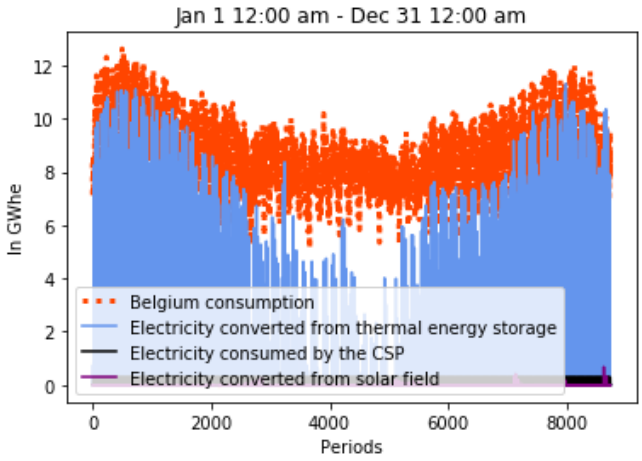

Figure 51: Evolution of the Belgian consumption, the electricity converted from the thermal energy discharged from TES of the CSP, converted by the thermal energy leaving from the solar field and consumed by the CSP over the entire year on the graph on the right from the optimization results using all production means

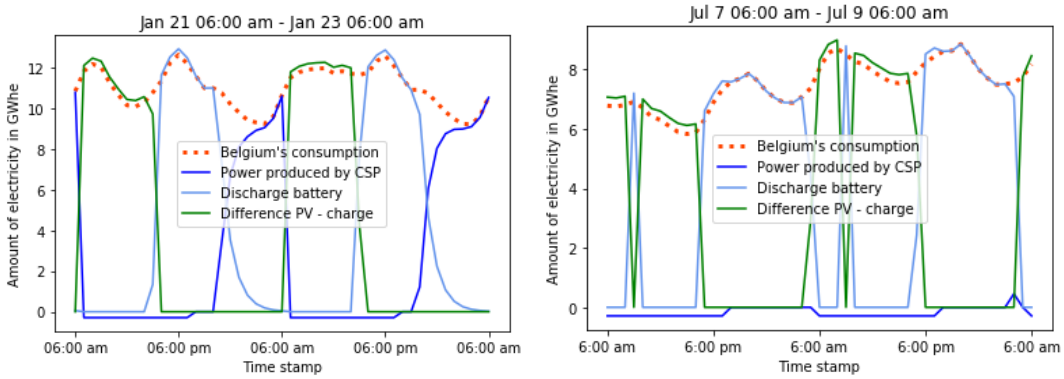

Figure 52: Evolution of the electricity produced by the CSP, the difference between the PV and the electricity charged in the battery storage (therefore, the part of the PV generation directly used to feed the load) and the electricity discharged from the battery storage along with Belgian demand from January 21^{st} to January 23^{rd} on the left graph and from July 7^{th} to July 9^{th} on the right graph from the optimization results using all production means

Despite the lower use of thermal storage and the increase in the LCOE related to the CSP, the LCOE of the entire installation is more advantageous than the LCOE when only the PV and the battery were used to meet the Belgium demand. From 91.28 $/MWh using only the PV-battery system, the cost was reduced to 77.74 $/MWh when adding the CSP within the assumptions of the model.

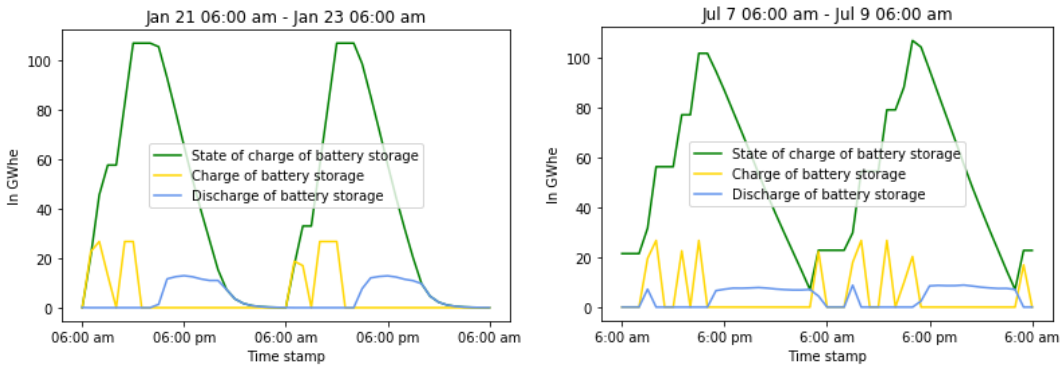

Figure 53: Evolution of the state of charge of the battery storage, the energy charged and the energy discharged from January 21^{st} to January 23^{rd} on the left graph and from July 7^{th} to July 9^{th} on the right graph from the optimization results using all production means

Part VII
Conclusion

The objective of this thesis was to determine if concentrated solar power (CSP) plants were still economically viable when put in competition with PV systems and batteries for a large scale power generation in a global grid setting. In order to establish this comparison, an optimization-based framework was implemented using results of simulations from the System Advisor Model (SAM) as a reference for modelling CSP and PVs and from scientific literature for electric battery. Data related with costs of technologies are taken from publications from the US National Renewable Energy Laboratory (NREL).

The configuration of the system considers Kôm Ombo in Egypt as the installation site and the Belgium electricity demand as load. Results of the optimization show that the LCOE, the levelized cost of electricity, decreases when CSP is added to the PV-battery system. Within an investment horizon of 25 years, the LCOE drops from 110.20 $/MWh using only PVs and battery to 77.74 $/MWh for the most realistic setting. The LCOE decrease is achieved by taking advantage of the thermal energy storage (TES) of the CSP which allow to generate electricity several hours after collecting energy through the solar field. These results clearly show that, under realistic capacity and cost assumptions, CSP may still be economically viable today, in particular by designing a system in which CSP and PV-battery systems play a complementary role.

Note that, in more futuristic scenarios where the thermal storage capacity of the CSP is not constrained by the model, CSP could even be used as the sole source of storage to further decrease the LCOE. Nonetheless, in this thesis, since costs are based on existing projects, constraints regarding the CSP capacity (generation and storage) were added in order to remain within a realistic frame. Therefore, further academic and industrial research should be conducted in order to better evaluate the cost decrease potential of designing CSP with much larger storage capacity.

Moreover, although the model was based on the results from the well-established software SAM, the results proposed in this thesis are being generate with a simplified version of SAM's output using linear regression as an approximation method. It could be interesting to evaluate the impact of these approximations on the tightness of the results in order to guide the improvement the model, but this is left for future research.

References

[1] World Energy Council(2016). *World Energy Scenarios 2016*. World Energy Council, London

[2] J. Yu, K. Bakic, A. Kumar, A. Iliceto, L. Beleke Tabu, J.L.Ruaud, J. Fan, B. Cova, H. Li, D. Ernst, R. Fonteneau, M. Theku, G. Sanchis, N. Chamollet, M. Le Du, Y. Zhang, S. Chatzivasileiadis, D. Radu, M. Berger, M. Stabile, F. Heymann, M.A. Dupre La Tour, M.M. De Villena, M. Ranjbar. (September 2019) *Global electricity network - Feasibility Study*

[3] IRENA (2017). *Electricity Storage and Renewables: Costs and Markets to 2030*

[4] S. Chatzivasileiadis, D. Ernst and G. Andersson (2013). *The Global Grid*. Renewable Energy, vol. 57, pp. 372-383

[5] Connaissance des énergies, *Desertec*. Accessed December 7, 2019. `https://www.connaissancedesenergies.org/fiche-pedagogique/desertec`.

[6] F. Trieb, M. O'Sullivan, T. Pregger, C. Schillings, W. Krewitt (July 2009). *Characterisation of Solar Electricity Import Corridors from MENA to Europe. Potential, Infrastructure and Cost*. German Aerospace Centre (DLR), Stuttgart, Germany

[7] J. Santamarta (2011). *Concentrated Solar Power (CSP) Vs Photovoltaic (PV)* HELIOSCSP. Accessed December 2, 2020. `http://helioscsp.com/concentrated-solar-power-csp-vs-photovoltaic-pv/#:~:text=Concentrated%20Solar%20Thermal%20systems%20(CSP,and%20drive%20an%20electric%20generator.`

[8] Selwa Calderbank (2013) *Desertec abandon Sahara solar power export dream* Euractiv. Accessed December 7, 2019. `https://www.euractiv.com/section/trade-society/news/desertec-abandons-sahara-solar-power-export-dream/`.

[9] *Key Requirements for Concentrating Solar Power (CSP) Plants*. Helioscsp. Accessed July 27, 2020 `http://helioscsp.com/key-requirements-for-concentrating-solar-power-csp-plants/`

[10] P. Dewallef (2019). *Slides à l'intention du cours de Renewable Energies*. Université de Liège. Liège, Belgique

[11] Tulu Wegayehu, Yonatan Mulushoa, N. Murali, and T. Arunamani (April 2017) *BRIEF REVIEW OF SOLID ELECTROLYTE FOR LITHIUM ION BATTERIES IN PARTICULAR TO GARNET-STRUCTURED...,*. ResearchGate.

[12] Michael J. Wagner and Paul Gilman (June 2011). *Technical Manual for the SAM Physical Trough Model.* National Renewable Energy Laboratory. Golden, Colorado, USA

[13] System Advisor Model Version 2020.2.29 (SAM 2020.2.29). National Renewable Energy Laboratory. Golden, Colorado, USA. Accessed April 16, 2020. `https://sam.nrel.gov/download`

[14] System Advisor Model Version 2017.9.5 (SAM 2017.9.5). User Documentation. Weather File Formats. National Renewable Energy Laboratory. Golden, Colorado, USA

[15] Photovoltaic Geographical Information System. European Commission. Accessed May 3, 2020. `https://re.jrc.ec.europa.eu/pvg_tools/en/tools.html`

[16] Salahuddin Qazi (2017). *Standalone Photovoltaic (PV) Systems for Disaster Relief and Remote Areas*

[17] International Renewable Energy Agency (IRENA) (June 2012). *Renewable energy technologies : cost analysis series. Concentrating Solar Power*

[18] Fichtner (2010). *Technology Assessment of CSP Technologies for a Site Specific Project in South Africa Final Report*. Washington DC.

[19] Jürgen Dersch, Michael Geyer,Ulf Herrmann,Scott A.Jones,Bruce Kelly,Rainer Kistner, Winfried Ortmanns, Robert Pitz-Paal, and Henry Price (2004). *Trough integration into power plants: A study on the performance and economy of integrated solar combined cycle systems.* Energy, 29:947–959

[20] C. Druet, M. Berger, B. Miftari, G. Detier (September 2020). *Generic System Modelling Language - Release 1.0.* University of Liege, Liege, Belgium

[21] Marco Binotti, Guangdong Zhu, Allison Gray, Giampaolo Manzolini, Paolo Silva. *Geometric analysis of three-dimensional effects of parabolic trough collectors*. Sol. Energy, 88 (2013), pp. 88-96

[22] Ener-T International. SEGS Projetcs. `https://www.enertgroup.net/projects`

[23] V.K.Jebasingh, G.M. JoselinHerbert. *A review of solar parabolic trough collector*

[24] Potential for solar thermal energy by country - Egypt. SolarPaces. Accessed July 27, 2020 `https://www.solarpaces.org/csp-technologies/csp-potential-solar-thermal-energy-by-member-nation/egypt/`

[25] Therminol VP-1 Heat Transfer Fluid. Eastman. Accessed July 30, 2020. `https://www.therminol.com/product/71093459`

[26] D. Kearney, B. Kelly, R. Cable, N. Potrovitza, U. Herrmann, P. Nava, R. Mahoney, J. Pacheco S, D. Blake, H. Price (February 20-21, 2003). *Overview on use of a Molten Salt HTF in a Trough Solar Field* National Renewable Energy Laboratory. Golden, Colorado, USA

[27] A. Azouzoutea, A. Alami Merrounia, M. Garoumb, E. G. Bennounaa. *Soiling loss of solar glass and mirror samples in the region with arid climate.* 6th International Conference on Energy and Environment Research, ICEER 2019, 22-25 July, University of Aveiro, Portugal

[28] *Kiewit:: Fixed-tilt vs. axis tracker solar panels.* Kiewit.com, 2013. Accessed December 14, 2020 `https://www.kiewit.com/plant-insider/current-issue/fixed-tilt-vs-axis-tracker-solar-panels/`

[29] Trading Economics. Belgium Inflation Rate. Accessed August 15, 2020. `https://tradingeconomics.com/belgium/inflation-cpi`

[30] Mecometer. Central bank discount rate - Belgium. Accessed August 15, 2020. `http://mecometer.com/whats/belgium/central-bank-discount-rate/`

[31] W. Cole and A. W. Frazier (June 2019). *Cost Projections for Utility-Scale Battery Storage*. National Renewable Energy Laboratory. Golden, Colorado, USA

[32] B. Cornelusse (2019). *Slides à l'intention du cours de Microgrid*. Université de Liège. Liège, Belgique

[33] Gurobi Optimization. https://www.gurobi.com/

[34] Elia. Grid data. Data Download. https://www.elia.be/en/grid-data/data-download-page

[35] X. Py, Najim Sadiki, Régis Olives, and Q. Falcoz (2017) *Thermal energy storage for CSP (Concentrating Solar Power)*, ResearchGate. Accessed December 29, 2020. https://www.researchgate.net/publication/318669304_Thermal_energy_storage_for_CSP_Concentrating_Solar_Power